Origin of circular dichroism in resonant elastic x-ray scattering from magnetic and polar chiral structures

Kook Tae Kim,[1] Jung Yun Kee,[1] Margaret R. McCarter,[2] Gerrit van der Laan,[3] Vladimir A. Stoica,[4,5] John W. Freeland,[4] Ramamoorthy Ramesh,[2,6,7] Se Young Park,[1,*] and Dong Ryeol Lee[1,†]

[1]*Department of Physics, Soongsil University, Seoul 06978, Korea*

[2]*Department of Physics, University of California, Berkeley, California 94720, USA*

[3]*Diamond Light Source, Harwell Science and Innovation Campus, Didcot, Oxfordshire OX11 0DE, United Kingdom*

[4]*Advanced Photon Source, Argonne National Laboratory, Lemont, Illinois 60439, USA*

[5]*Department of Materials Science and Engineering, The Pennsylvania State University, State College, Pennsylvania 16802, USA*

[6]*Department of Materials Science and Engineering, University of California, Berkeley, Berkeley, California 94720, USA*

[7]*Materials Sciences Division, Lawrence Berkeley National Laboratory, Berkeley, California 94720, USA*

(Received 3 March 2022; revised 19 May 2022; accepted 27 June 2022; published 11 July 2022)

Circular dichroism in resonant elastic x-ray scattering (CD-REXS) has recently been observed in chiral structures composed of multiferroic materials as well as magnetic moments or electric polarization vectors. In order to comprehensively understand the experimental results of these previous studies, we present here in detail the analytical formulation of CD-REXS for one-dimensional helices composed of magnetic moments and electric polarization vectors, respectively. In particular, by comparing CD-REXS for a proper-screw-shaped Bloch-type helix and cycloid-shaped Néel-type helix, we found that CD-REXS for both magnetic and polar helices can discriminate between both types of helices. We also found that the x-ray polarization factor depending on the scattering geometry is a significant factor in determining the characteristics of CD-REXS for chiral structures. The results obtained from the detailed formulas can be intuitively understood using the concept of mirror reflection. In particular, in this way it can be understood that Bloch- and Néel-type helices correspond to truly chiral and achiral structures, respectively, and why CD-REXS is able to distinguish between these two types of helices.

DOI: 10.1103/PhysRevB.106.035116

I. INTRODUCTION

Chirality is an important and interesting topic in physics, chemistry, and biology. Since chiral structures are either right- and left-handed, whether their presence is balanced forms one of the most fascinating topics. The chiral structure that has recently attracted the most attention in condensed-matter physics is the skyrmion, with a complicated topological pattern. In the case of a magnetic skyrmion in the form of spirals of continuously rotating spin magnetic moments, many studies are being conducted for future spintronic applications because of topological stability and possible manipulation with very low electrical current densities [1–5]. In addition, polar skyrmions composed of electric polarization vectors corresponding to the electrical counterparts were also recently experimentally discovered [6]. Probing the complicated chiral textures of these skyrmions is not only necessary to understand their mechanism but is also a very challenging research topic in itself.

A well-known method to experimentally characterize magnetic or polar chiral textures is resonant elastic x-ray scattering (REXS) [7]. According to the unique x-ray polarization dependence of the scattering amplitude of REXS, for a chiral structure it shows circular dichroism (CD), in which the scattering intensities of right- and left-circularly polarized x rays are different [8–14]. In particular, satellite peaks with diffraction orders of opposite sign (Friedel pairs) show a reversed sign of the CD. Also, if the handedness of the chiral structure is reversed, the sign of the CD is reversed. If these characteristics are observed in CD in REXS (CD-REXS), the material is highly likely to have a chiral structure. Therefore the use of CD-REXS is gradually becoming prominent in the investigation of the chiral structure of electric polarization vectors observed in ferroelectric oxide superlattices [15,16], as well as the chiral magnetic structures observed in skyrmions [10–12,17] or magnetic domain walls [8,9]. However, since the overall understanding of CD-REXS on polar and magnetic chiral structures is deficient, it remains challenging to understand why CD-REXS changes depending on the sign of the diffraction order and the handedness of the chiral structure.

In this paper we present the analytical formulation of CD-REXS for one-dimensional (1D) helices in detail to clearly show how CD appears in the chiral structure. To this end, we first show that a truly chiral structure like a proper-screw-type helix and an achiral structure like a cycloid-type helix are feasible by comparing their mirrored helices. In the case of magnetic moments, these two chiral structures correspond

*sp2829@ssu.ac.kr
†drlee@ssu.ac.kr

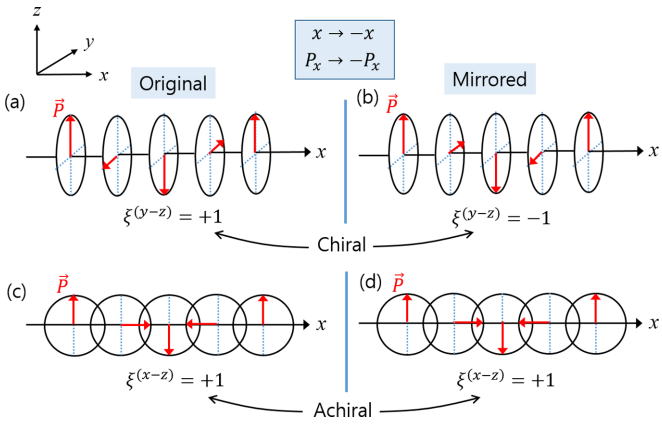

FIG. 1. One-dimensional helices consisting of electric polarization vectors with (y-z) and (x-z) plane rotations and their mirrored helices. Under the mirror reflection along the x axis, the sign of the x component of the electric polarization vector $\vec{P}$ is reversed. True chiral structure is not superimposed with its mirror image by translation or rotation. A proper-screw-type (a) helix is truly chiral and has opposite handedness as its mirrored helix (b). The handedness ξ of the helix is denoted as positive when rotating clockwise in positive direction of the propagation axis. On the other hand, a cycloid-type (c) helix is achiral and has the same handedness as its mirrored counterpart (d).

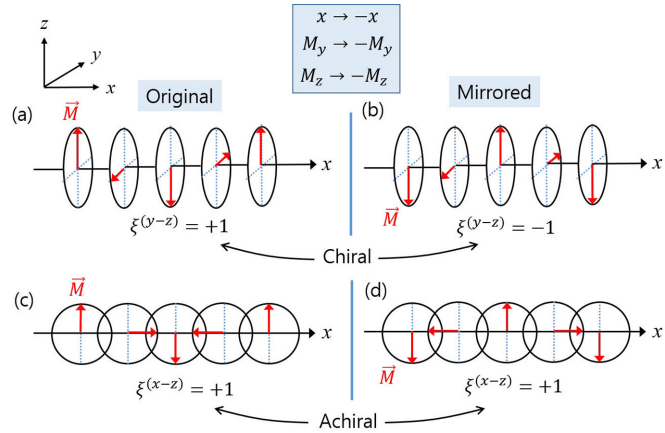

FIG. 2. One-dimensional helices consisting of magnetic moments with (y-z) and (x-z) plane rotations and their mirrored helices. Under the mirror reflection along the x axis, the signs of the y and z components of the magnetic moment $\vec{M}$ are reversed. A proper-screw-type (a) helix is truly chiral and has the opposite sign of handedness as its mirrored helix (b). On the other hand, a cycloid-type (c) helix is achiral and has the same handedness as its mirrored counterpart (d).

to Bloch- and Néel-type domain walls, respectively, and in the case of electric polarization vectors, both of these chiral structures can be found in the polar vortex or polar skyrmion expressed in the ferroelectric superlattice [6,18–21]. We use mirror reflection to show that these two helices correspond to truly chiral and achiral structures, respectively, and for both electric polarization vector and magnetic moment cases, CD-REXS can discriminate between these two types of helices. In particular, unlike the magnetic moment explicitly included in the resonant scattering amplitude [7], for the electric polarization vector the REXS is calculated in the form of the anisotropy tensor of susceptibility [22,23], so a theoretical calculation method was only recently published [16]. Therefore there have only been a few studies comparing the REXS for the two electric and magnetic 1D helices, and here we compare the two cases to enhance the overall understanding of the CD-REXS for the chiral structure. To this end, we present a detailed analytical formulation to calculate the CD-REXS intensity for both cases. In addition, the change in CD-REXS for scattering geometries with different methods of accessing satellite peaks diffracted from 1D helices of periodic array type is also examined in detail. Finally, we show that the CD-REXS for 1D helices and their mirrored helices are all consistent for these various cases.

II. CHIRALITY IN 1D HELICES

We consider here two types of 1D helix, namely, proper-screw- and cycloid-type helices. When the helix propagates along the x axis, the polarization vector or magnetic moment rotates in the (y-z) and (z-x) planes, respectively, as shown in Figs. 1 and 2. The former corresponds to a Bloch-type domain wall in ferromagnetic domains, while the latter corresponds to a Néel-type domain wall. According to the definition of chirality, a structure is said to be chiral when it cannot be superimposed with the original shape by any translation or rotation after mirror reflection. Figure 1 shows mirror images for helices composed of electric polarization vectors. In the case of the polarization vector $\vec{P}$, which is an electric dipole (polar vector), if a mirror is normal to the x axis, the P_x components must be $-P_x$. A Bloch-type helix of (y-z) plane rotation is a "chiral" structure because the handedness of the helix is reversed after mirror reflection and the mirrored and original helices are not superimposable onto each other. Note that the handedness ξ of the helix is denoted as positive when rotating clockwise in positive direction of the propagation axis. On the other hand, a Néel-type helix of (x-z) plane rotation does not change the handedness of the helix after mirror reflection and is therefore an "achiral" structure because the mirrored helix can be superimposed with the original one.

Figure 2 shows the mirror reflections for helices consisting of magnetic moments, which are axial vectors. If the mirror reflection is taken along the x axis for the magnetic moment $\vec{M}$ of the magnetic dipole, the M_y and M_z components will be $-M_y$ and $-M_z$, respectively. The Bloch-type magnetic helix of the (y-z) plane rotation also has a "chiral" structure because the handedness is reversed after mirror reflection and cannot be superimposed onto the original helix. On the other hand, in the Néel-type helix of (x-z) plane rotation, the handedness of the helix does not change after mirror reflection. The helix of (x-z) plane rotation is "achiral" because the original and mirror helices are superimposable onto each other when translated along the x axis. In summary, for both electric polarization vectors and magnetic moments, the Bloch- and Néel-type helices correspond to truly chiral and achiral structures, respectively. Zhang *et al.* already showed that ordered spin spiral structures can be fully determined in a single measurement by CD-REXS [24], which was subsequently used

to distinguish between Bloch- and Néel-type skyrmions and to determine the helicity angle of twisted surface skyrmions [12]. Chauleau *et al*. presented a distinction between Bloch- and Néel-type magnetic domain walls using CD-REXS [11]. In this paper we comprehensively present how CD-REXS can distinguish between these chiral and achiral structures for both polar and magnetic chiral configurations.

III. SCATTERING AMPLITUDES IN REXS

A. Scattering amplitude for a resonant atom

In the electric-dipole approximation, in which dipole transitions between the core state $|\zeta_v\rangle$ with energy E_v and the unoccupied valence state $|\psi_\eta\rangle$ with E_η are present in both the absorption and emission channel, the resonant scattering amplitude from a resonant atom can be written as [25]

$$f_{\text{res}}(E) = \sum_{ij} \epsilon_i' \epsilon_j \sum_{\eta} \frac{\langle \zeta_v | R_i | \psi_\eta \rangle \langle \psi_\eta | R_j | \zeta_v \rangle}{E - (E_\eta - E_v) + i\Gamma} = \sum_{ij} \epsilon_i' \epsilon_j T_{ij}, \tag{1}$$

where ϵ_i' and ϵ_j in the polarization factor are the components of unit polarization vectors for scattered and incident x rays, respectively. R is the position operator. When the resonant atom has a parity-even magnetic moment $\hat{M}$, assuming cylindrical symmetry, the amplitude can be expressed as follows in an explicit form with respect to $\hat{M}$ [7,14]:

$$f_{\text{res, mag}}(E) = (\hat{\epsilon}' \cdot \hat{\epsilon}) f_0(E) - i(\hat{\epsilon}' \times \hat{\epsilon}) \cdot \hat{M} f_1(E) + (\hat{\epsilon}' \cdot \hat{M})(\hat{\epsilon} \cdot \hat{M}) f_2(E). \tag{2}$$

On the other hand, in the case of a polarization vector which is parity-odd, the dipole-dipole resonant scattering amplitude is parity-even as in Eq. (1), so it cannot be expressed in this form. As in Eq. (1), the anisotropic tensor (AT) T_{ij} must be obtained directly. Instead, we first choose a resonant atom at a specific position as the basis atom with diagonal matrix elements so that its AT can be easily calculated using its site symmetry in the crystal. The ATs of the remaining resonant atoms having a polarization vector in an arbitrary direction can then be obtained using the rotation of the AT of the basis atom. For example, in ferroelectric ABO_3 perovskites, we can choose a B-site ion having $\vec{P}_0$ polarization along the $\pm\hat{c}$-axis direction as the basis atom. In this case, since the basis atom such as the Ti^{4+} ion in $PbTiO_3$ has a fourfold rotational symmetry about the $\hat{c}$ axis and mirror symmetry about the $\hat{a}$ and $(\hat{a} + \hat{b})$ axes, its AT $\boldsymbol{T}_0$ has the simple form

$$\boldsymbol{T}_0 = \begin{pmatrix} T_{xx} & 0 & 0 \\ 0 & T_{xx} & 0 \\ 0 & 0 & T_{zz} \end{pmatrix}. \tag{3}$$

Since the polarization vector $\vec{P}_n = \mathcal{R}(\phi_{n,x}, \phi_{n,z})\vec{P}_0$ of the remaining resonant atoms is obtained by rotating the basis vector $\vec{P}_0$ about the x and z axis by the angles $\phi_{n,x}$ and $\phi_{n,z}$, respectively, where $\mathcal{R}$ is the rotation matrix, its corresponding AT $\boldsymbol{T}_n$ can be expressed by [26]

$$\boldsymbol{T}_n = \mathcal{R}(\phi_{n,x}, \phi_{n,z}) \boldsymbol{T}_0 \mathcal{R}(\phi_{n,x}, \phi_{n,z})^T, \tag{4}$$

where $\mathcal{R}^T$ denotes a transpose of $\mathcal{R}$. One point worth noting is that the AT T_{ij} defined in Eq. (1) can be divided into irreducible parts as follows [25]:

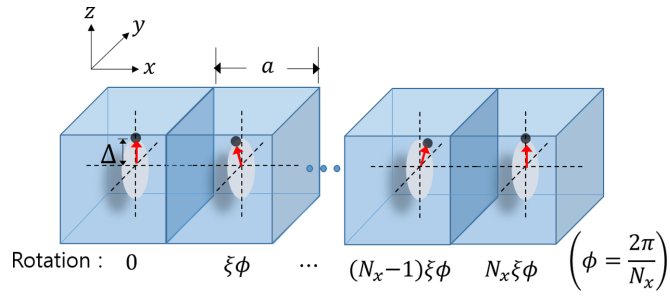

FIG. 3. Schematic drawing of a unit cell of a 1D helix with electric polarization vectors due to the displacement of resonant atoms from the unit-cell center. N_x is the number of lattices in a unit cell of the helix, Δ is the magnitude of the displacement of the resonant atom, and ξ is the handedness of the helix. At each position the resonant atom rotates by $\xi\phi$.

$$T_{ij} = \tfrac{1}{3}\,\text{tr}\,(T_{ij})\delta_{ij} + T_{ij}^A + T_{ij}^S$$
$$T_{ij}^A = \tfrac{1}{2}(T_{ij} - T_{ji}),\ T_{ij}^s = \tfrac{1}{2}\big(T_{ij} + T_{ji} - \tfrac{2}{3}\delta_{ij}\,\text{tr}\,(T_{ij})\big), \tag{5}$$

where $\text{tr}(T_{ij})$ is the trace term summing over all diagonal components, T_{ij}^A is an antisymmetric tensor, and T_{ij}^S is a traceless symmetric tensor. For a magnetic moment and with cylindrical symmetry, T_{ij}^A corresponds to the second term of Eq. (2). However, if there is no magnetic moment, T_{ij}^A vanishes and only the symmetric tensor remains. Therefore the AT of Eqs. (3) and (4) for the polarization vector always corresponds to a symmetric tensor, satisfying $T_{ij} = T_{ji}$.

B. Structure factor of 1D helices

The structure factor F_{helix} for the unit cell of the 1D helix is

$$F_{\text{helix}} = \sum_{n=0}^{N_x-1} e^{i\vec{q}\cdot\vec{r}_n} f_{\text{res},n} = \sum_{ij} \epsilon_i' \epsilon_j \sum_{n=0}^{N_x-1} e^{i\vec{q}\cdot\vec{r}_n} (T_n)_{ij}, \tag{6}$$

where N_x is the number of lattices in the unit cell of the helix.

1. Electric polarization vectors

The electric polarization vector appears due to the displacement of the resonant ion from the center of the surrounding ions with opposite charge, so when calculating the structure factor for the 1D helix of the unit cell, the displacement of the resonant ion must be considered. As shown in Fig. 3, if the displacement is Δ and it rotates by $\xi\phi$ in the (y-z) plane for each resonant ion position, $\vec{r}_n = [na, \Delta\sin(n\xi\phi), \Delta\cos(n\xi\phi)]$ in the phase factor of Eq. (6), where ξ is the handedness of the helix. This helix corresponds to a Bloch- or proper-screw-type helix, which is truly chiral. Since we discuss here how CD-REXS appears at the lateral satellite peak due to the period of the 1D helix along the x axis, we only deal with the case where $\vec{q} = (2\pi\tau/(N_x a), 0, q_z)$ in Eq. (6). τ is the diffraction order of the satellite along the q_x axis. Then, for the case where the polarization vector rotates in the (y-z) plane, the structure

factor in Eq. (6) is given as

$$F_{\text{helix}}^{(y\text{-}z)} = \sum_{ij} \epsilon_i' \epsilon_j \frac{1}{N_x} \sum_{n=0}^{N_x-1} e^{i[\tau\phi n + q_z \Delta \cos(n\xi\phi)]} \times \mathcal{R}_x(-n\xi\phi)(T_0)_{ij}\mathcal{R}_x^T(-n\xi\phi). \quad (7)$$

Since the magnitude of the displacement of the resonant atom, Δ, in ferroelectric perovskites is an order of magnitude smaller than the lattice parameter [18], $q_z\Delta$ in the soft x-ray regime, where typical CD-REXS experiments are conducted, is sufficiently small ($q_z\Delta \ll 1$). Equation (7) can be then approximated as $e^{iq_z\Delta\cos(n\xi\phi)} \approx 1 + iq_z\Delta\cos(n\xi\phi)$, so it can be expressed by

$$F_{\text{helix}}^{(y\text{-}z)} \approx \sum_{ij} \epsilon_i' \epsilon_j \frac{1}{N_x} \sum_{n=0}^{N_x-1} e^{i\tau\phi n}\left(1 + \frac{iq_z\Delta}{2}(e^{in\xi\phi} + e^{-in\xi\phi})\right) \times \mathcal{R}_x(-n\xi\phi)(T_0)_{ij}\mathcal{R}_x^T(-n\xi\phi). \quad (8)$$

When the matrix component of the AT $\boldsymbol{T}_0$ of the basis atom in Eq. (8) is simply expressed as $T_{ij}(i, j = x, y, z)$ from now on, the AT for the (y-z) plane rotation, $\boldsymbol{T}^{(y\text{-}z)} = \mathcal{R}_x(-n\xi\phi)\boldsymbol{T}_0\mathcal{R}_x^T(-n\xi\phi)$, can be expressed as

$$\begin{aligned}
T_{xx}^{(y\text{-}z)} &= T_{xx},\\
T_{yy}^{(y\text{-}z)} &= T_{yy}\cos^2(n\xi\phi) + T_{zz}\sin^2(n\xi\phi)\\
&\quad - 2T_{yz}\sin(n\xi\phi)\cos(n\xi\phi),\\
T_{zz}^{(y\text{-}z)} &= T_{yy}\sin^2(n\xi\phi) + T_{zz}\cos^2(n\xi\phi)\\
&\quad + 2T_{yz}\sin(n\xi\phi)\cos(n\xi\phi),\\
T_{xy}^{(y\text{-}z)} &= T_{yx}^{(y\text{-}z)} = T_{xy}\cos(n\xi\phi) - T_{xz}\sin(n\xi\phi),\\
T_{xz}^{(y\text{-}z)} &= T_{zx}^{(y\text{-}z)} = T_{xy}\sin(n\xi\phi) + T_{xz}\cos(n\xi\phi),\\
T_{yz}^{(y\text{-}z)} &= T_{zy}^{(y\text{-}z)} = (T_{yy} - T_{zz})\cos(n\xi\phi)\sin(n\xi\phi)\\
&\quad + T_{yz}\cos(2n\xi\phi).
\end{aligned} \quad (9)$$

Here, since the AT is for a polarization vector without a magnetic moment, there is no antisymmetric tensor term in Eq. (5) and the AT is a symmetric tensor, so $T_{ij} = T_{ji}$ for all its components. Since the AT $\boldsymbol{T}^{(y\text{-}z)}$ in Eq. (9) always includes a trigonometric function, Eq. (8) always has the form $e^{in\phi x}$ for all matrix components. In this case, if N_x is sufficiently large, the following relational expression can be considered:

$$\frac{1}{N_x}\sum_{n=0}^{N_x-1} e^{in\phi x} = \frac{1}{N_x}\sum_{n=0}^{N_x-1} e^{i\frac{2\pi}{N_x}nx} \cong \delta(x). \quad (10)$$

Introducing the helix-only structure factor S_{ij} excluding the x-ray polarization factor $\epsilon_i'\epsilon_j$, the structure factor in Eq. (8) is expressed by

$$F_{\text{helix}} = \sum_{ij} \epsilon_i' \epsilon_j S_{ij}. \quad (11)$$

Then $S_{ij}^{(y\text{-}z)}$ for the (y-z) plane rotation is given by

$$S_{ij}^{(y\text{-}z)} \approx \frac{1}{N_x}\sum_{n=0}^{N_x-1} e^{i\tau\phi n}\left(1 + \frac{iq_z\Delta}{2}(e^{in\xi\phi} + e^{-in\xi\phi})\right)T_{ij}^{(y\text{-}z)}. \quad (12)$$

Looking at Eq. (9) by components, first of all, the diagonal components $T_{xx}^{(y\text{-}z)}$, $T_{yy}^{(y\text{-}z)}$, and $T_{zz}^{(y\text{-}z)}$ consist of only terms that include $e^{(\pm 2in\xi\phi)}$ or have no relation to $(n\xi\phi)$. Therefore, considering the $e^{i\tau\phi n}$ factor in Eq. (12), all $S_{xx}^{(y\text{-}z)}$, $S_{yy}^{(y\text{-}z)}$, and $S_{zz}^{(y\text{-}z)}$ must have $\delta(\tau)$ or $\delta(\tau \pm 2)$ according to Eq. (10). However, since the $e^{i\tau\phi n}$ factor in Eq. (12) is actually $e^{i\tau\phi n}[1 + \frac{iq_z\Delta}{2}(e^{in\xi\phi} + e^{-in\xi\phi})]$, $\delta(\tau)$ and $\delta(\tau \pm 2)$ should be replaced with $\delta_\xi^{(y\text{-}z)}(\tau)$ and $\delta_\xi^{(y\text{-}z)}(\tau \pm 2\xi)$ when $\delta_\xi^{(y\text{-}z)}(x)$ is expressed in a simpler form as

$$\delta_\xi^{(y\text{-}z)}(x) \equiv \delta(x) + i\left(\frac{q_z\Delta}{2}\right)\{\delta(x+\xi) + \delta(x-\xi)\}. \quad (13)$$

On the other hand, among the off-diagonal components of Eq. (9), $T_{xy}^{(y\text{-}z)}(= T_{yx}^{(y\text{-}z)})$ and $T_{xz}^{(y\text{-}z)}(= T_{zx}^{(y\text{-}z)})$ include the term $e^{(\pm in\xi\phi)}$, so $S_{xy}^{(y\text{-}z)}(= S_{yx}^{(y\text{-}z)})$ and $S_{xz}^{(y\text{-}z)}(= S_{zx}^{(y\text{-}z)})$ contain only the term $\delta_\xi^{(y\text{-}z)}(\tau \pm \xi)$. However, since $T_{yz}^{(y\text{-}z)}(= T_{zy}^{(y\text{-}z)})$ related to the (y-z) rotation plane includes the term $e^{(\pm 2in\xi\phi)}$, $S_{yz}^{(y\text{-}z)}(= S_{zy}^{(y\text{-}z)})$ in Eq. (12) includes only the $\delta_\xi^{(y\text{-}z)}(\tau \pm 2\xi)$ term. Finally, $S_{ij}^{(y\text{-}z)}$ for the (y-z) plane rotation can be described for each matrix component as

$$\begin{aligned}
S_{xx}^{(y\text{-}z)} &= T_{xx}\delta_\xi^{(y\text{-}z)}(\tau),\\
S_{yy}^{(y\text{-}z)} &= \frac{1}{4}\{2T_0\delta_\xi^{(y\text{-}z)}(\tau) + T_{2+}\delta_\xi^{(y\text{-}z)}(\tau + 2\xi)\\
&\quad + T_{2-}\delta_\xi^{(y\text{-}z)}(\tau - 2\xi)\},\\
S_{zz}^{(y\text{-}z)} &= \frac{1}{4}\{2T_0\delta_\xi^{(y\text{-}z)}(\tau) - T_{2+}\delta_\xi^{(y\text{-}z)}(\tau + 2\xi)\\
&\quad - T_{2-}\delta_\xi^{(y\text{-}z)}(\tau - 2\xi)\},\\
S_{xy}^{(y\text{-}z)} &= S_{yx}^{(y\text{-}z)} = \frac{1}{2}\{T_{1+}\delta_\xi^{(y\text{-}z)}(\tau + \xi) + T_{1-}\delta_\xi^{(y\text{-}z)}(\tau - \xi)\},\\
S_{xz}^{(y\text{-}z)} &= S_{zx}^{(y\text{-}z)} = \frac{1}{2i}\{T_{1+}\delta_\xi^{(y\text{-}z)}(\tau + \xi) - T_{1-}\delta_\xi^{(y\text{-}z)}(\tau - \xi)\},\\
S_{yz}^{(y\text{-}z)} &= S_{zy}^{(y\text{-}z)} = \frac{1}{4i}\{T_{2+}\delta_\xi^{(y\text{-}z)}(\tau + 2\xi) - T_{2-}\delta_\xi^{(y\text{-}z)}(\tau - 2\xi)\},
\end{aligned} \quad (14)$$

where T_0, $T_{(1\pm)}$, and $T_{(2\pm)}$ are defined as

$$\begin{aligned}
T_0 &\equiv T_{yy} + T_{zz},\\
T_{1+} &\equiv T_{xy} + iT_{xz},\\
T_{1-} &\equiv T_{xy} - iT_{xz},\\
T_{2+} &\equiv T_{yy} - T_{zz} + 2iT_{yz},\\
T_{2-} &\equiv T_{yy} - T_{zz} - 2iT_{yz}.
\end{aligned} \quad (15)$$

From Eqs. (13)–(15), two special situations can be considered: (i) when there is no displacement of the polarization vector ($\Delta = 0$), and (ii) when the off-diagonal components of the AT of the basis atom are all zero due to crystal symmetry as in Eq. (3) [$T_{ij}(i \neq j) = 0$]. We only deal with the second case, which is more practical, below. (Refer to Appendix A for the first case.) If there are no off-diagonal components as in Eq. (3), since $T_{1\pm} = 0$ in Eq. (15), $S_{xy}^{(y\text{-}z)} = S_{yx}^{(y\text{-}z)} = S_{xz}^{(y\text{-}z)} = S_{zx}^{(y\text{-}z)} = 0$ in Eq. (14). On the other hand, $T_{2\pm} = T_{yy} - T_{zz}$.

Now, since we are interested in CD-REXS of the first-order satellite among the lateral satellite peak τ, consider only the

case where $\tau = \pm\xi$. In this case, only the terms including $\delta(\tau \pm \xi)$ in Eq. (14) need to be considered. As mentioned above, considering the zero off-diagonal components, the helix-only structure factor in Eq. (14) is reduced as follows when $\tau = \pm\xi$:

$$\begin{aligned} S_{xx}^{(y\text{-}z)} &= (iA)T_{xx}, \\ S_{yy}^{(y\text{-}z)} &= \tfrac{1}{4}(iA)(3T_{yy} + T_{zz}), \\ S_{zz}^{(y\text{-}z)} &= \tfrac{1}{4}(iA)(T_{yy} + 3T_{zz}), \\ S_{xy}^{(y\text{-}z)} &= S_{yx}^{(y\text{-}z)} = S_{xz}^{(y\text{-}z)} = S_{zx}^{(y\text{-}z)} = 0, \\ S_{yz}^{(y\text{-}z)} &= S_{zy}^{(y\text{-}z)} = \mp\tfrac{1}{4}A(T_{yy} - T_{zz}) = (-\tau\xi)\tfrac{1}{4}A(T_{yy} - T_{zz}), \end{aligned} \tag{16}$$

where $A \equiv (q_z\Delta)/2$, and the upper and lower signs correspond to the cases of $\tau = +\xi$ and $\tau = -\xi$, respectively, and $(\pm)$ can be expressed as $(\tau\xi)$ when the first-order satellite peaks ($\tau = \pm 1$) are considered. In Eq. (16), we should note two things. First, all $S_{ij}^{(y\text{-}z)}$ terms include a factor A proportional to the displacement Δ. When analyzing CD-REXS measured in the experiment, the asymmetry ratio (AR) $[= (I_+ - I_-)/(I_+ + I_-)]$ obtained by dividing the difference intensity CD $(= I_+ - I_-)$ by the sum intensity is used most frequently. $I_\pm$ corresponds to the scattering intensities for right- and left-circular x rays, respectively. Since the factor A cancels out in the denominator and numerator, quantitative analysis is possible without detailed information on the magnitude of the displacement.

The next thing to note is that only $S_{yz}^{(y\text{-}z)} = S_{zy}^{(y\text{-}z)}$ has a $(\tau\xi)$ dependence associated with chirality. This $(\tau\xi)$ dependence is a well-known characteristic of CD-REXS for chiral structures. That is, when the sign of the diffraction order of the satellite peak is reversed ($\tau = \pm 1$) or the sign of the handedness of the helix is reversed ($\xi = \pm 1$), it can be expected that the sign of the CD is changed. However, among the terms $S_{ij}^{(y\text{-}z)}$, the reason that only $S_{yz}^{(y\text{-}z)} = S_{zy}^{(y\text{-}z)}$ has $(\tau\xi)$ dependence is because the polarization vector rotates in the $(y\text{-}z)$ plane. Therefore it can be expected that these results will be similar to the other type of helix shown in Fig. 1. That is, does the $(\tau\xi)$ dependence appear only in $S_{xz}^{(x\text{-}z)} = S_{zx}^{(x\text{-}z)}$ also for a cycloid-type helix rotating in the $(x\text{-}z)$ plane? To answer this, we present now the REXS structure factor for a Néel- or cycloid-type helix.

Similar to a Bloch- or proper-screw-type helix shown in Fig. 3, if there is a rotation by $\xi\phi$ in the $(x\text{-}z)$ plane at each resonant atom position, $\vec{r}_n = [na + \Delta\sin(n\xi\phi), 0, \Delta\cos(n\xi\phi)]$ is given in the phase factor of Eq. (6). This helix corresponds to a Néel- or cycloid-type helix, which is achiral. Therefore the structure factor of Eq. (6) can be written as

$$\begin{aligned} F_{\text{helix}}^{(x\text{-}z)} = \sum_{ij} \epsilon_i' \epsilon_j \frac{1}{N_x} \sum_{n=0}^{N_x-1} e^{i[\tau\phi n + \frac{\Delta}{a}\tau\phi\sin(n\xi\phi) + q_z\Delta\cos(n\xi\phi)]} \\ \times \mathcal{R}_y(-n\xi\phi)(T_0)_{ij}\mathcal{R}_y^T(-n\xi\phi). \end{aligned} \tag{17}$$

Since the size of the unit cell of the helix is typically about 10 nm in polar vortices and polar skyrmions [6,18], the number of lattices in the unit cell of the helix N_x corresponds to about a few tens for ferroelectric perovskites, and $\phi(= 2\pi/N_x)$ is smaller than unity. The exponent $[\frac{\Delta}{a}\tau\phi\sin(n\xi\phi) + q_z\Delta\cos(n\xi\phi)]$ is then sufficiently small in the phase factor of Eq. (17) and can be approximated as

$$\begin{aligned} e^{i(\tau\phi n + \frac{\Delta}{a}\tau\phi\sin(n\xi\phi) + q_z\Delta\cos(n\xi\phi))} &\approx e^{i\tau\phi n}\left[1 + i\left(\frac{\Delta}{a}\tau\phi\right)\sin(n\xi\phi) + i(q_z\Delta)\cos(n\xi\phi)\right] \\ &= e^{i\tau\phi n}\left[1 + e^{in\xi\phi}\left(\frac{1}{2}\frac{\Delta}{a}\tau\phi + \frac{i}{2}q_z\Delta\right) + e^{-in\xi\phi}\left(-\frac{1}{2}\frac{\Delta}{a}\tau\phi + \frac{i}{2}q_z\Delta\right)\right]. \end{aligned} \tag{18}$$

In Eq. (18), $(\frac{\Delta}{a}\tau\phi)$ is sufficiently small compared to $(q_z\Delta)$, $(\tau\phi \ll q_z a)$, and Eq. (17) can be expressed as

$$\begin{aligned} F_{\text{helix}}^{(x\text{-}z)} \approx \sum_{ij} \epsilon_i' \epsilon_j \frac{1}{N_x} \sum_{n=0}^{N_x-1} e^{i\tau\phi n}\left(1 + \frac{iq_z\Delta}{2}(e^{in\xi\phi} + e^{-in\xi\phi})\right) \\ \times \mathcal{R}_y(-n\xi\phi)(T_0)_{ij}\mathcal{R}_y^T(-n\xi\phi). \end{aligned} \tag{19}$$

Equation (19) has the same form as Eq. (8) in the case of y-z plane rotation, except that it is $\mathcal{R}_y$, which is a rotation about the y axis, instead of $\mathcal{R}_x$, which is a rotation about the x axis. Therefore, if we substitute according to $(x \to y, y \to z, z \to x)$ from Eqs. (13)–(16) described for the case of y-z plane rotation, all of them correspond to the case of x-z plane rotation. It should be noted that in the definition of T_0, $T_{1\pm}$, and $T_{2\pm}$ in Eq. (15), substitution should be also made according to $(x \to y, y \to z, z \to x)$. However, the definition of Eq. (13) is the same, so $\delta_\xi^{(x\text{-}z)}(x) = \delta_\xi^{(y\text{-}z)}(x)$.

When the AT of the basis atom has zero off-diagonal components, the helix-only structure factor $S_{ij}^{(x\text{-}z)}$ of the $(x\text{-}z)$ plane rotation when $\tau = \pm\xi$ is

$$\begin{aligned} S_{xx}^{(x\text{-}z)} &= \tfrac{1}{4}(iA)(T_{zz} + 3T_{xx}), \\ S_{yy}^{(x\text{-}z)} &= (iA)T_{yy}, \\ S_{zz}^{(x\text{-}z)} &= \tfrac{1}{4}(iA)(3T_{zz} + T_{xx}), \\ S_{xy}^{(x\text{-}z)} &= S_{yx}^{(x\text{-}z)} = S_{yz}^{(x\text{-}z)} = S_{zy}^{(x\text{-}z)} = 0, \\ S_{zx}^{(x\text{-}z)} &= S_{xz}^{(x\text{-}z)} = \mp\tfrac{1}{4}A(T_{zz} - T_{xx}) = (-\tau\xi)\tfrac{1}{4}A(T_{zz} - T_{xx}), \end{aligned} \tag{20}$$

where $A \equiv (q_z\Delta)/2$, upper and lower signs correspond to $\tau = +\xi$ and $\tau = -\xi$, respectively, and $(\pm)$ can be expressed by $(\tau\xi)$. Finally, we confirm that $(\tau\xi)$ dependence appears only in $S_{xz}^{(x\text{-}z)} = S_{xz}^{(x\text{-}z)}$ also for a cycloid-type helix rotating in the $(x\text{-}z)$ plane. As discussed above in Fig. 1, true chirality appears only in the case of $(y\text{-}z)$ plane rotation of a Bloch-type helix,

whereas the $(\tau\xi)$ dependence is common to all helices, so it seems not suitable as a criterion for classifying true chirality.

2. Magnetic moments

In the case of magnetic moments, there is no displacement of the resonant atom, and the scattering amplitude has the form of Eq. (2). By virtue of the optical theorem the second term in Eq. (2) can be related to the x-ray magnetic circular dichroism (XMCD) in absorption. The third term in the scattering is quadratic in $\hat{M}$, related to the x-ray magnetic linear dichroism (XMLD), and is proportional to the anisotropy in the spin-orbit interaction, which is directly related to the magnetocrystalline anisotropy energy [27]. Since the spin-orbit interaction is strongly reduced by the crystalline field in $3d$ ferromagnetic metals, the third term is usually much smaller. Considering only the first and second terms, the structure factor in REXS from the 1D helix in which the magnetic moment rotates can be described as

$$F_{\text{helix}}^{\text{mag}} = \frac{1}{N_x}\sum_{n=0}^{N_x-1} e^{i\tau\phi n}((\hat{\epsilon}'\cdot\hat{\epsilon})f_c - i(\hat{\epsilon}'\times\hat{\epsilon})\cdot\hat{M}(n\xi\phi)f_m), \tag{21}$$

where the energy-dependent resonant scattering amplitudes $f_0(E)$ and $f_1(E)$ have been replaced with $f_c(E)$ and $f_m(E)$ to emphasize that the first and second terms of Eq. (2) correspond to purely charge and magnetic contributions, respectively. The photon energy is taken at resonance in this study, and no explicit mention of the energy dependence of f_c and f_m will be used hereafter. In Eq. (21), the term proportional to f_c simply has $(\hat{\epsilon}'\cdot\hat{\epsilon})f_c\delta(\tau)$ according to the relational expression of Eq. (10). Considering this, the structure factor of Eq. (21) can be expressed as

$$F_{\text{helix}}^{\text{mag}} = (\hat{\epsilon}'\cdot\hat{\epsilon})f_c\delta(\tau) - i(\hat{\epsilon}'\times\hat{\epsilon})\cdot\widetilde{\mathbf{M}}(\tau,\xi)f_m, \tag{22}$$

where the helix-only structure factor $\widetilde{\mathbf{M}}(\tau,\xi)$ is defined by

$$\widetilde{\mathbf{M}}(\tau,\xi) = \frac{1}{N_x}\sum_{n=0}^{N_x-1} e^{i\tau\phi n}\hat{M}(n\xi\phi). \tag{23}$$

As shown in Figs. 2 and 3, $\hat{M}(n\xi\phi) = [0, -\sin(n\xi\phi), \cos(n\xi\phi)]$ for a Bloch- or proper-screw-type helix whose magnetic moment rotates in the $(y\text{-}z)$ plane. The nonzero components $\widetilde{\mathrm{M}}_i^{(y\text{-}z)}$ in Eq. (23) are given by

$$\begin{aligned}
\widetilde{\mathrm{M}}_y^{(y\text{-}z)} &= \frac{1}{N_x}\sum_{n=0}^{N_x-1} e^{i\tau\phi n}[-\sin(n\xi\phi)] \\
&= \frac{1}{N_x}\sum_{n=0}^{N_x-1} e^{i\tau\phi n}\left(\frac{i}{2}\right)\left(e^{in\xi\phi} - e^{-in\xi\phi}\right), \\
\widetilde{\mathrm{M}}_z^{(y\text{-}z)} &= \frac{1}{N_x}\sum_{n=0}^{N_x-1} e^{i\tau\phi n}\cos(n\xi\phi) \\
&= \frac{1}{N_x}\sum_{n=0}^{N_x-1} e^{i\tau\phi n}\left(\frac{1}{2}\right)\left(e^{in\xi\phi} + e^{-in\xi\phi}\right).
\end{aligned} \tag{24}$$

Using the relational expression of Eq. (10), Eq. (24) can be expressed by

$$\begin{aligned}
&\widetilde{\mathrm{M}}_x^{(y\text{-}z)} = 0, \quad \widetilde{\mathrm{M}}_y^{(y\text{-}z)} = \left(\frac{i}{2}\right)[\delta(\tau+\xi) - \delta(\tau-\xi)], \\
&\widetilde{\mathrm{M}}_z^{(y\text{-}z)} = \left(\frac{1}{2}\right)[\delta(\tau+\xi) + \delta(\tau-\xi)].
\end{aligned} \tag{25}$$

When $\tau = \pm\xi$ corresponding to the first-order satellite peak, the first term of Eq. (22) is zero and Eq. (25) is reduced as follows:

$$\widetilde{\mathrm{M}}_x^{(y\text{-}z)} = 0, \quad \widetilde{\mathrm{M}}_y^{(y\text{-}z)} = \mp\left(\frac{i}{2}\right) = -(\tau\xi)\left(\frac{i}{2}\right), \quad \widetilde{\mathrm{M}}_z^{(y\text{-}z)} = \frac{1}{2}, \tag{26}$$

where the upper and lower signs correspond to the cases of $\tau = +\xi$ and $\tau = -\xi$, respectively, and $(\pm)$ can be expressed as $(\tau\xi)$. It can be seen that only $\widetilde{\mathrm{M}}_y^{(y\text{-}z)}$ and $\widetilde{\mathrm{M}}_z^{(y\text{-}z)}$ components on the y-z plane in which the magnetic moment rotates are nonzero, and one of them always has $(\tau\xi)$ dependence and the other has a constant value. Is this result the same for a Néel- or cycloid-type helix rotating in the $(x\text{-}z)$ plane?

Similar to a Bloch-type helix shown in Fig. 3, $\hat{M}(n\xi\phi) = [\sin(n\xi\phi), 0, \cos(n\xi\phi)]$ for a Néel-type helix whose magnetic moment rotates in the $(x\text{-}z)$ plane. Its helix-only structure factor $\widetilde{\mathrm{M}}_i^{(x\text{-}z)}$ is then given by

$$\begin{aligned}
&\widetilde{\mathrm{M}}_x^{(x\text{-}z)} = -\left(\frac{i}{2}\right)[\delta(\tau+\xi) - \delta(\tau-\xi)], \quad \widetilde{\mathrm{M}}_y^{(x\text{-}z)} = 0, \\
&\widetilde{\mathrm{M}}_z^{(x\text{-}z)} = \left(\frac{1}{2}\right)[\delta(\tau+\xi) + \delta(\tau-\xi)].
\end{aligned} \tag{27}$$

When $\tau = \pm\xi$, Eq. (27) is reduced as follows:

$$\widetilde{\mathrm{M}}_x^{(x\text{-}z)} = \pm\left(\frac{i}{2}\right) = (\tau\xi)\left(\frac{i}{2}\right), \widetilde{\mathrm{M}}_y^{(x\text{-}z)} = 0, \quad \widetilde{\mathrm{M}}_z^{(x\text{-}z)} = \frac{1}{2}, \tag{28}$$

where the upper and lower signs correspond to $\tau = +\xi$ and $\tau = -\xi$, respectively, and $(\pm)$ can be expressed as $(\tau\xi)$. We confirm that only $\widetilde{\mathrm{M}}_x^{(x\text{-}z)}$ and $\widetilde{\mathrm{M}}_z^{(x\text{-}z)}$ components on the $(x\text{-}z)$ plane in which the magnetic moment rotates are nonzero, and one of them always has $(\tau\xi)$ dependence and the other has a constant value. Therefore, as in the case of S_{ij} for the electric polarization vector, the helix-only structure factor $\widetilde{\mathrm{M}}_i$ of the 1D helicity of the magnetic moment is not sufficient to distinguish the true chirality.

C. X-ray polarization factor in scattering amplitude

Previously, we presented the structure factors in REXS from Bloch- or Néel-type helices with electric polarization vectors or magnetic moments. However, it is found that for both polar and magnetic helices, the helix-only structure factors are not sufficient to distinguish between truly chiral and achiral structures. Here we investigate the x-ray polarization factor $\hat{\epsilon}_i'\hat{\epsilon}_j$ in Eq. (6), which is also a significant part in the structure factor in REXS.

The x-ray polarization factor depends entirely on the scattering geometry. The most frequently used scattering geometry in recent soft x-ray resonant scattering experiments is a sample-fixed mode using a two-dimensional (2D) detector. This method is widely used in grazing-incidence small-angle

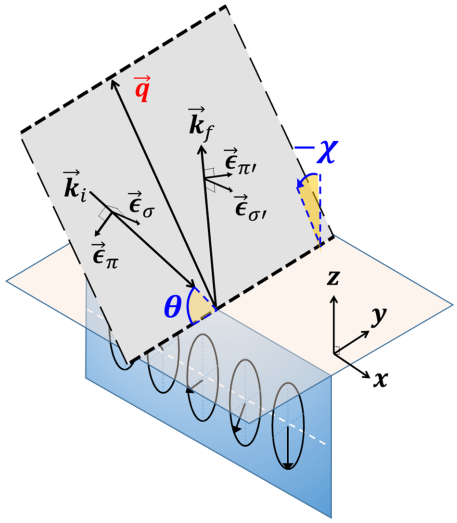

FIG. 4. Sample-tilting (azimuthal-fixed) scattering geometry. The angles θ and χ represent the incident and the tilting angle, respectively.

x-ray scattering (GISAXS)[28–31] and has the advantage of effectively reducing the measurement time. However, in GISAXS using a 2D detector, effectively both sample-rocking and azimuthal scans occur simultaneously, so it is suitable for nanostructured thin films with random orientation in the in-plane direction. However, the sample-fixed mode using a 2D detector is not an optimal method to study epitaxial thin films with clear ordering in the in-plane direction. In particular, in the case of the 1D helix dealt with in this paper, the lateral satellite peak must be accessed while maintaining the direction of the propagation axis of the helix, and the q_z rod scan must be performed in the direction of the surface normal. For this, two scattering geometries, namely, sample-tilting and sample-rocking scattering geometry, can be used. The former is a method to obtain the q_x value in the in-plane direction by fixing the azimuthal angle and tilting the sample with respect to the scattering plane as shown in Fig. 4. On the other hand, the latter is a method to obtain the q_x value by fixing the detector angle and rocking the sample as shown in Fig. 5. This

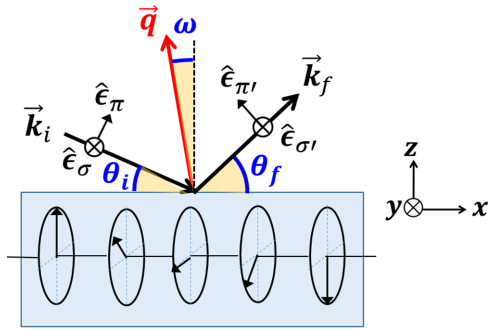

FIG. 5. Sample-rocking scattering geometry. The in-plane component of $\vec{q}$ is given by the angle $\omega = (\theta_i - \theta_f)/2$, where θ_i and θ_f are the incident and scattered angles, respectively.

method is well known as rocking curve scan. Here, the x-ray polarization factor of the structure factor in REXS from 1D helices for these two scattering geometries will be calculated in detail.

1. Sample tilting (azimuthal-fixed) scattering geometry

The unit polarization vectors for scattered and incident x rays in the sample-tilting scattering geometry, $\hat{\epsilon}'$ and $\hat{\epsilon}$, are as follows for the σ and π channels as shown in Fig. 4:

$$\begin{aligned}
\hat{\epsilon}'_\sigma &= (\cos\chi, 0, -\sin\chi),\\
\hat{\epsilon}'_\pi &= (-\cos\theta\sin\chi, \sin\theta, -\cos\theta\cos\chi),\\
\hat{\epsilon}_\sigma &= \hat{\epsilon}'_\sigma,\\
\hat{\epsilon}_\pi &= (-\cos\theta\sin\chi, -\sin\theta, -\cos\theta\cos\chi).
\end{aligned} \tag{29}$$

The structure factor in REXS from the 1D helix of the electric polarization vectors can be obtained for each polarization channel by using Eqs. (11) and (29) as

$$\begin{aligned}
F_{\sigma'\sigma} &= \cos^2\chi\ S_{xx} + \sin^2\chi\ S_{zz} - 2\cos\chi\sin\chi\ S_{xz'},\\
F_{\sigma'\pi} &= \cos\theta\cos\chi\sin\chi\ (S_{zz} - S_{xx}) - \sin\theta\cos\chi\ S_{xy}\\
&\quad + \sin\theta\sin\chi\ S_{yz} - \cos\theta\cos 2\chi\ S_{xz},\\
F_{\pi'\sigma} &= \cos\theta\cos\chi\sin\chi\ (S_{zz} - S_{xx}) + \sin\theta\cos\chi\ S_{xy}\\
&\quad - \sin\theta\sin\chi\ S_{yz} - \cos\theta\cos 2\chi\ S_{xz},\\
F_{\pi'\pi} &= \cos^2\theta\sin^2\chi\ S_{xx} - \sin^2\theta\ S_{yy} + \cos^2\theta\cos^2\chi\ S_{zz}\\
&\quad + 2\cos^2\theta\cos\chi\sin\chi\ S_{xz},
\end{aligned} \tag{30}$$

where the subscript of the structure factor $F_{\alpha'\beta}$ represents the polarization channels of scattered and incident x rays, respectively. Previously, it has been shown that the helix-only structure factor S_{ij} has $(\tau\xi)$ dependence only in components related to the rotation plane of the helix. For example, in the case of a helix rotating in the $(y\text{-}z)$ plane, only the $S_{yz} = S_{zy}$ component has $(\tau\xi)$ dependence. On the other hand, the x-ray polarization factors in Eq. (30) show an explicit τ dependence additionally. In Eq. (30), $\sin\chi$, which is an odd function for χ angle, changes according to the sign of the diffraction order τ of the lateral satellite peak, so $\sin\chi$ can be expressed as $\tau|\sin\chi|$ at the first-order satellites ($\tau = \pm\xi$). Interestingly, in Eq. (30), the terms odd for χ are allowed only in the terms containing S_{xx}, S_{zz}, S_{xz}, and S_{yz}.

The structure factor in REXS from the 1D helix consisting of magnetic moments can be obtained for each polarization channel by using Eqs. (22) and (29) as

$$\begin{aligned}
F_{\sigma'\sigma} &= 0,\\
F_{\sigma'\pi} &= f_m(-\sin\theta\sin\chi\ \widetilde{\mathrm{M}}_x + \cos\theta\ \widetilde{\mathrm{M}}_y - \sin\theta\cos\chi\ \widetilde{\mathrm{M}}_z),\\
F_{\pi'\sigma} &= f_m(-\sin\theta\sin\chi\ \widetilde{\mathrm{M}}_x - \cos\theta\ \widetilde{\mathrm{M}}_y - \sin\theta\cos\chi\ \widetilde{\mathrm{M}}_z),\\
F_{\pi'\pi} &= f_m(-\sin 2\theta\cos\chi\ \widetilde{\mathrm{M}}_x + \sin 2\theta\sin\chi\ \widetilde{\mathrm{M}}_z).
\end{aligned} \tag{31}$$

Here, the first term in Eq. (22), which contributes only to the zeroth-order peak, is excluded. A constant factor $(-i)$ in the second term of Eq. (22) is also factored out. In the sample-tilting scattering geometry, the sign of the tilting angle χ should be reversed to reverse the sign of the diffraction order τ of the lateral satellite peak, so all odd functions for

χ angle such as $\sin\chi$ have a τ dependence. The x-ray polarization factors in Eq. (31) then show an explicit τ dependence additionally. Interestingly, in Eq. (31), the terms odd for χ are allowed only in the terms containing $\widetilde{\mathrm{M}}_x$ and $\widetilde{\mathrm{M}}_z$.

2. *Sample rocking scattering geometry*

The unit polarization vectors for the sample-rocking scattering geometry are as follows for the σ and π channels in Fig. 5:

$$\begin{aligned}&\hat{\epsilon}'_\sigma = (0,1,0), \quad \hat{\epsilon}'_\pi = (-\sin\theta_f, 0, \cos\theta_f),\\ &\hat{\epsilon}_\sigma = \hat{\epsilon}'_\sigma, \quad \hat{\epsilon}_\pi = (\sin\theta_i, 0, \cos\theta_i).\end{aligned} \tag{32}$$

In this case, the structure factor in REXS from the electric polarization vectors is as follows for each polarization channel according to Eqs. (11) and (32):

$$\begin{aligned}F_{\sigma'\sigma} &= S_{yy},\\ F_{\sigma'\pi} &= \sin\theta_i\, S_{xy} + \cos\theta_i\, S_{yz},\\ F_{\pi'\sigma} &= -\sin\theta_f\, S_{xy} + \cos\theta_f\, S_{yz},\\ F_{\pi'\pi} &= \sin 2\omega\, S_{xz} + \cos\theta_i \cos\theta_f\, S_{zz},\end{aligned} \tag{33}$$

where $\omega = (\theta_i - \theta_f)/2$, and as shown in Fig. 5, when the sign of ω is changed, the sign of the diffraction order τ of the lateral satellite peak is reversed. Therefore only terms that are odd in ω have τ dependence, and in Eq. (33) the terms containing S_{xz} correspond to this case.

The structure factor in REXS from magnetic moments is as follows for each polarization channel according to Eqs. (22) and (32):

$$\begin{aligned}F_{\sigma'\sigma} &= 0,\\ F_{\sigma'\pi} &= f_m(-\cos\theta_i\, \widetilde{\mathrm{M}}_x - \sin\theta_i\, \widetilde{\mathrm{M}}_z),\\ F_{\pi'\sigma} &= f_m(-\cos\theta_f\, \widetilde{\mathrm{M}}_x - \sin\theta_f\, \widetilde{\mathrm{M}}_z),\\ F_{\pi'\pi} &= f_m \sin(\theta_i + \theta_f)\, \widetilde{\mathrm{M}}_y.\end{aligned} \tag{34}$$

Here, there is no ω dependence that can change the sign of the diffraction order τ.

IV. CIRCULAR DICHROISM IN REXS FROM 1D HELICES

CD in REXS can be obtained with scattering amplitudes of σ and π channel as [32]

$$I_+ - I_- = 2\,\mathrm{Im}[F^*_{\sigma'\pi}F_{\sigma'\sigma} + F^*_{\pi'\pi}F_{\pi'\sigma}]. \tag{35}$$

A. Electric polarization vectors

The detailed evaluation of Eq. (35) using Eq. (30), which is the calculated REXS structure factor for the electric polarization vectors in the sample-tilting scattering geometry, is shown in Eq. (B1) in Appendix B. First we discuss a Bloch-type helix that rotates in the (y-z) plane. When all off-diagonal components of the AT $\boldsymbol{T}_0$ for the basis atom are zero, the helix-only structure factor $S^{(y\text{-}z)}_{ij}$ in Eq. (16) for the first-order satellite ($\tau = \pm\xi$) is applied to Eq. (B1) in Appendix B, and CD- REXS is then given by

$$\begin{aligned}&\frac{(I_+ - I_-)}{2}\\ &= \frac{3A^2}{2}\,\mathrm{Im}[T^*_{zz}T_{xx}](\cos\theta\sin^2\theta\cos\chi)\sin\chi\\ &\pm \frac{A^2}{4^2}|T_{xx}|^2(3\sin^2\theta\sin^2\chi + \sin^2\theta - 5)\sin\theta\sin\chi\\ &\pm \frac{A^2}{4^2}|T_{zz}|^2(3\sin^2\theta\sin^2\chi - 4\sin^2\theta + 3)\sin\theta\sin\chi\\ &\pm \frac{A^2}{8}\,\mathrm{Re}[T^*_{zz}T_{xx}](-3\sin^2\theta\sin^2\chi + 1)\sin\theta\sin\chi.\end{aligned} \tag{36}$$

As discussed in the previous sections, $\sin\chi$, an odd function for the χ angle, can be expressed as $\tau|\sin\chi|$ for the first-order satellite ($\tau = \pm\xi$). In addition, since the sign ($\pm$) can be expressed by ($\tau\xi$), Eq. (36) can be expressed as

$$(I_+ - I_-)^{(y\text{-}z)} = \tau\mathcal{A}^{(y\text{-}z)} + \tau(\tau\xi)\mathcal{B}^{(y\text{-}z)} = \tau\mathcal{A}^{(y\text{-}z)} + \xi\mathcal{B}^{(y\text{-}z)}, \tag{37}$$

where the terms $\mathcal{A}^{(y\text{-}z)}$ and $\mathcal{B}^{(y\text{-}z)}$ are independent of both the diffraction order τ and the handedness of the helix ξ. This is an unexpected result different from that of previous studies of CD-REXS on the chiral structure stating that the sign of CD-REXS is reversed when the handedness of the chiral structure is reversed or the sign of the diffraction order is reversed. According to Eq. (37), even when the sign of the diffraction order τ is reversed, the CD-REXS intensity does not simply change sign, and when the second term of Eq. (37) is dominant, the sign of the CD-REXS intensity may not change.

Next, CD-REXS for a Néel-type helix rotating in the (x-z) plane for the first-order satellite ($\tau = \pm\xi$) can be obtained by applying Eq. (20) to Eq. (B1) in Appendix B and is given by

$$\begin{aligned}&\frac{(I_+ - I_-)}{2}\\ &= A^2\,\mathrm{Im}[T^*_{zz}T_{xx}](\cos\theta\sin^2\theta\cos\chi)\sin\chi\\ &\pm \frac{A^2}{4^2}|T_{xx}|^2(12\sin^2\theta\sin^2\chi - 5\sin^2\theta - 2)\cos\theta\\ &\pm \frac{A^2}{4^2}|T_{zz}|^2(-4\sin^2\theta\sin^2\chi + 3\sin^2\theta - 2)\cos\theta\\ &\pm \frac{A^2}{8}\,\mathrm{Re}[T^*_{zz}T_{xx}](-4\sin^2\theta\sin^2\chi + \sin^2\theta + 2)\cos\theta.\end{aligned} \tag{38}$$

In the sample-tilting scattering geometry, ($\sin\chi$) and ($\pm$) can be expressed as $\tau|\sin\chi|$ and ($\tau\xi$), respectively, for the first-order satellite ($\tau = \pm\xi$). Equation (38) can be then expressed as

$$(I_+ - I_-)^{(x\text{-}z)} = \tau\mathcal{A}^{(x\text{-}z)} + (\tau\xi)\mathcal{D}^{(x\text{-}z)}, \tag{39}$$

where the terms $\mathcal{A}^{(x\text{-}z)}$ and $\mathcal{D}^{(x\text{-}z)}$ are independent of both the diffraction order τ and handedness of the helix ξ. Unlike Eq. (37) for the Bloch-type helix discussed above, the result of Eq. (39) for the Néel-type helix is consistent with that

of previous studies, where the CD-REXS intensity is exactly reversed in sign when the sign of the diffraction order τ is reversed.

Now, the results of Eqs. (37) and (39) make it possible to distinguish a Bloch-type helix of (y-z) rotation showing true chirality from a Néel-type helix of (x-z) rotation corresponding to achiral structure, as shown in Fig. 1. This is different from the previous result that the helix-only structure factor S_{ij} does not discriminate between these two helix types. Considering these results, it has been revealed that the main cause for CD-REXS to distinguish the true chirality is the x-ray polarization factor in a specific scattering geometry. These results are also the same for CD-REXS for helix of magnetic moment, which will be discussed later.

The key characteristics of CD-REXS from chiral structures is that the sign of the CD is reversed when the chirality of the material, which corresponds to the helix handedness ξ here, is reversed or when measured from a satellite peak whose diffraction order τ is opposite. This characteristics corresponds to the case where CD-REXS is proportional to $(\tau\xi)$, and the helix-only structure factor S_{ij} has been found to contain this $(\tau\xi)$ dependence for both Bloch- and Néel-type helices, regardless of true chirality. However, the x-ray polarization factor in the sample-tilting scattering geometry changes the $(\tau\xi)$ dependence of the helix-only structure factor S_{ij} to ξ dependence of the CD-REXS only for the Bloch-type helix of the (y-z) rotation showing true chirality. Therefore, according to Eq. (37), two satellite peaks having opposite signs of diffraction order τ may have the same sign of CD intensities and may not replicate each other when one of them is upside down, even though they have the opposite sign. On the other hand, for the Néel-type helix rotating in the (x-z) plane without true chirality, according to Eq. (39), the CD intensities at two satellite peaks having opposite signs of diffraction order τ exactly replicate when one of them is upside down.

Considering the mirrored images as shown in Fig. 1, we can understand the results of Eqs. (37) and (39) more clearly. First, the mirrored image of the x-ray beams in the sample-tilting scattering geometry can be considered, as shown in Fig. 6. In the mirrored image of the scattering geometry where the sign of q_x is reversed, the sign of the diffraction order τ of the lateral satellite is then reversed. In the case of a Bloch-type helix of (y-z) plane rotation with $\xi = +1$ at the satellite peak with $\tau = +1$, the CD intensity is $(I_+ - I_-)^{(y\text{-}z)} = \mathcal{A}^{(y\text{-}z)} + \mathcal{B}^{(y\text{-}z)}$ according to Eq. (37). In its mirrored situation, since $\tau = -1$ and $\xi = -1$, the CD intensity is then $(I_+ - I_-)^{(y\text{-}z)} = -(\mathcal{A}^{(y\text{-}z)} + \mathcal{B}^{(y\text{-}z)})$. On the other hand, in the case of a Néel-type helix of a (x-z) plane rotation with $\xi = +1$ at the satellite peak with $\tau = +1$, the CD intensity is $(I_+ - I_-)^{(x\text{-}z)} = \mathcal{A}^{(x\text{-}z)} + \mathcal{D}^{(x\text{-}z)}$ according to Eq. (39). In its mirrored situation, $\tau = -1$, but $\xi = +1$ as shown in Fig. 1, so the CD intensity is $(I_+ - I_-)^{(x\text{-}z)} = -(\mathcal{A}^{(x\text{-}z)} + \mathcal{D}^{(x\text{-}z)})$. These results are summarized in Table I.

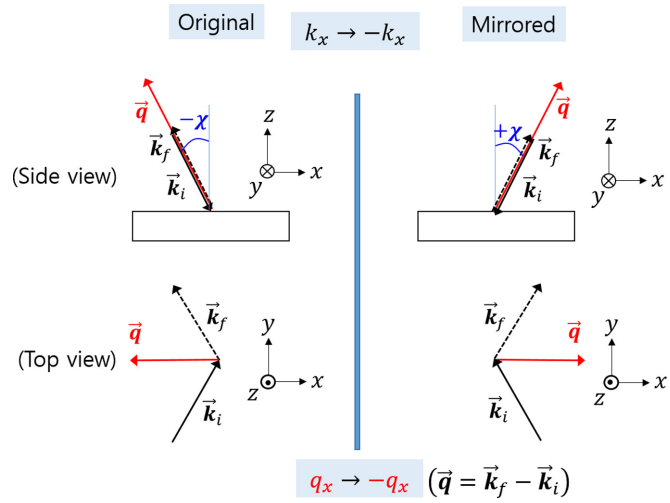

FIG. 6. Original (left panel) and mirrored (right panel) images of sample-tilting scattering geometry. Under the mirror reflection along the x axis, the signs of the x components of the wave vector $\vec{k}$ and the scattering vector $\vec{q}$ are reversed, and then the sign of the diffraction order τ is reversed.

Interestingly, in both the (y-z) and (x-z) plane rotation cases, the CD intensities in the mirrored condition show a reversed sign of those in the original condition. This can also be understood in terms of a mirrored situation of the circularly polarized x rays. Figure 7 shows that when circularly polarized x rays are mirrored along the x axis, the helicity (or handedness) of circular polarization in the mirrored situation is reversed compared to the original situation. Therefore, regardless of the type of helix, the sign of the CD intensity in the mirrored situation should be opposite to that of the original. As will be discussed later, this also applies to the helix of magnetic moments.

Next, the detailed evaluation of Eq. (35) using Eq. (33), which is the calculated REXS structure factor for the electric polarization vectors in the sample-rocking scattering geometry, is shown in Eq. (C1) in Appendix C. First we discuss a Bloch-type helix that rotates in the (y-z) plane. When all off-diagonal components of the AT $\boldsymbol{T}_0$ for the basis atom

TABLE I. Summary of the diffraction order τ, handedness ξ, and circular dichroism intensities for the original and mirrored helices with electric polarization vectors in the sample-tilting scattering geometry. Equations (37) and (39) correspond to Bloch-type and Néel-type helices, respectively.

	Original	Mirrored
Sample-tilting scattering geometry	$\tau = +1$	$\tau = -1$
Bloch-type helix with (y-z) plane rotation	$\xi = +1$	$\xi = -1$
$(I_+ - I_-)^{(y\text{-}z)} = \tau\mathcal{A}^{(y\text{-}z)} + \xi\mathcal{B}^{(y\text{-}z)}$ (Eq. (37))	$\mathcal{A}^{(y\text{-}z)} + \mathcal{B}^{(y\text{-}z)}$	$-(\mathcal{A}^{(y\text{-}z)} + \mathcal{B}^{(y\text{-}z)})$
Néel-type helix with (x-z) plane rotation	$\xi = +1$	$\xi = +1$
$(I_+ - I_-)^{(x\text{-}z)} = \tau\mathcal{A}^{(x\text{-}z)} + (\tau\xi)\mathcal{D}^{(x\text{-}z)}$ [Eq. (39)]	$\mathcal{A}^{(x\text{-}z)} + \mathcal{D}^{(x\text{-}z)}$	$-(\mathcal{A}^{(x\text{-}z)} + \mathcal{D}^{(x\text{-}z)})$

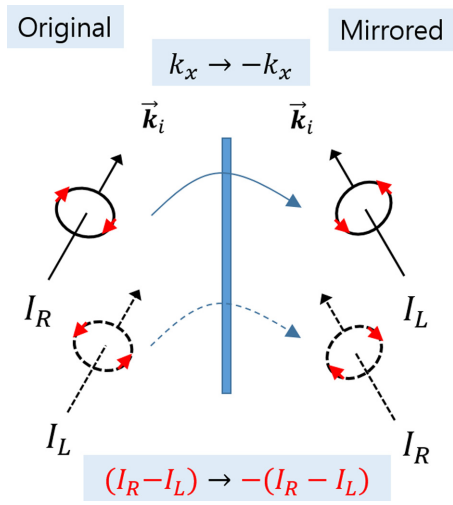

FIG. 7. Mirrored image of circularly polarized x rays. Under the mirror reflection along the x axis, the sign of circular polarization is reversed.

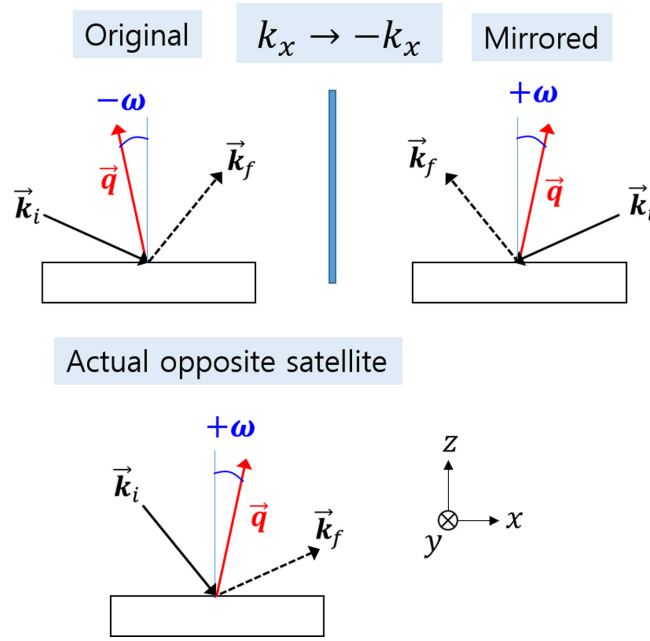

FIG. 8. Original (upper-left panel) and mirrored (upper-right panel) images of sample-rocking scattering geometry. Under the mirror reflection along the x axis, the signs of the x components of the wave vector $\vec{k}$ and the scattering vector $\vec{q}$ are reversed. However, the mirrored situation of sample-rocking scattering is different from the actual scattering configuration (bottom panel), where the sign of the diffraction order τ of the lateral satellite peak is reversed.

are zero, the helix-only structure factor $S_{ij}^{(y\text{-}z)}$ in Eq. (16) for the first-order satellite ($\tau = \pm\xi$) is applied to Eq. (C1) in Appendix C, and CD- REXS is then given by

$$\begin{aligned}\frac{(I_+ - I_-)}{2} = &\pm\frac{A^2}{4^2}|T_{xx}|^2(-3\cos\theta_i - 4\sin\theta_i\sin\theta_f\cos\theta_f \\ &+ \cos\theta_i\cos^2\theta_f) \pm \frac{A^2}{4^2}|T_{zz}|^2 \\ &\times(\cos\theta_i - 3\cos\theta_i\cos^2\theta_f) \\ &\pm\frac{A^2}{8}\mathrm{Re}[T_{zz}^* T_{xx}](\cos\theta_i + 2\sin\theta_i\sin\theta_f\cos\theta_f \\ &+ \cos\theta_i\cos^2\theta_f). \end{aligned} \tag{40}$$

As shown in Fig. 5, in order to reverse the sign of the diffraction order at the first-order satellite ($\tau = \pm\xi$) in the sample-rocking scattering geometry, there should be an odd function for the angle ω [$= (\theta_i - \theta_f)/2$], but it does not appear in Eq. (40). Since ($\pm$) can be expressed by ($\tau\xi$) at the first-order satellite ($\tau = \pm\xi$), Eq. (40) can be expressed as

$$(I_+ - I_-)_{\text{rock}}^{(y\text{-}z)} = (\tau\xi)\mathcal{D}_{\text{rock}}^{(y\text{-}z)}, \tag{41}$$

where the term $\mathcal{D}_{\text{rock}}^{(y\text{-}z)}$ is independent of both the diffraction order τ and the handedness of the helix ξ. Similarly, CD-REXS for a Néel-type helix rotating in the (x-z) plane for the first-order satellite ($\tau = \pm\xi$) can be obtained by applying Eq. (20) to Eq. (C1) in Appendix C and is then given by

$$(I_+ - I_-)_{\text{rock}}^{(x\text{-}z)} = 0, \tag{42}$$

because all terms in Eq. (C1) contain $S_{xy}^{(x\text{-}z)} = S_{yx}^{(x\text{-}z)} = S_{yz}^{(x\text{-}z)} = S_{zy}^{(x\text{-}z)} = 0$ in Eq. (20).

Equations (41) and (42) show that in the sample-rocking scattering geometry, the Bloch-type helix of (y-z) plane rotation has a ($\tau\xi$) dependence in CD-REXS intensity, while the Néel-type helix of the (x-z) plane rotation has no CD in REXS. This result allows the sample-rocking scattering geometry to discriminate between truly chiral Bloch-type and achiral Néel-type helices through CD-REXS intensity. However, as shown in Fig. 8, the mirror situation of sample-rocking scattering is different from the actual scattering geometry that reverses the sign of the diffraction order τ of the lateral satellite peak. Therefore it is difficult to apply the analysis using the mirror situation as discussed earlier in the sample-tilting scattering geometry. One further interesting result is that in the sample-rocking scattering geometry, CD in REXS is zero in the case of a helix in which the electric polarization vector rotates in the (x-z) plane corresponding to the scattering plane. The same is true for the magnetic moments, which will be discussed later.

B. Magnetic moments

The detailed evaluation of Eq. (35) using Eq. (31), which is the calculated REXS structure factor for magnetic moments in the sample-tilting scattering geometry, is given by

$$\begin{aligned}\frac{(I_+ - I_-)}{2} = &|f_m|^2(\sin 2\theta\cos\theta\cos\chi\ \ \mathrm{Im}[\widetilde{\mathrm{M}}_x^*\widetilde{\mathrm{M}}_y] \\ &+ \sin 2\theta\sin\theta\ \ \mathrm{Im}[\widetilde{\mathrm{M}}_x^*\widetilde{\mathrm{M}}_z] \\ &- \sin 2\theta\cos\theta\sin\chi\ \ \mathrm{Im}[\widetilde{\mathrm{M}}_z^*\widetilde{\mathrm{M}}_y]). \end{aligned} \tag{43}$$

First we discuss a Bloch-type helix that rotates in the (y-z) plane. When all off-diagonal components of the AT $\boldsymbol{T}_0$ for the basis atom are zero and the magnetic structure factor $\widetilde{\mathrm{M}}_i^{(y\text{-}z)}$ of Eq. (26) for the first-order satellite ($\tau = \pm\xi$) is applied to

Eq. (43), the CD- REXS is given as

$$\frac{I_+ - I_-}{2} = \pm\frac{1}{4}|f_m|^2 \sin 2\theta \cos\theta \sin\chi. \tag{44}$$

In the sample-tilting scattering geometry, $\sin\chi$ and $(\pm)$ can be expressed as $\tau|\sin\chi|$ and $(\tau\xi)$, respectively, for the first-order satellite ($\tau = \pm\xi$). Equation (44) can be expressed as

$$(I_+ - I_-)^{(y\text{-}z)}_{\text{mag}} = \tau(\tau\xi)\mathcal{B}^{(y\text{-}z)}_{\text{mag}} = \xi\mathcal{B}^{(y\text{-}z)}_{\text{mag}}, \tag{45}$$

where the term $\mathcal{B}^{(y\text{-}z)}_{\text{mag}}$ is independent of both the diffraction order τ and the handedness of the helix ξ. The result of Eq. (45) shows that the CD-REXS intensity for the Bloch-type helix of magnetic moments in the sample-tilting scattering geometry does not change its sign or magnitude even when the sign of the diffraction order is reversed.

Next, CD-REXS for a Néel-type helix rotating in the (x-z) plane for the first-order satellite ($\tau = \pm\xi$) can be obtained by applying Eq. (28) to Eq. (43) and is then given as

$$\frac{I_+ - I_-}{2} = \mp\frac{1}{4}|f_m|^2 \sin 2\theta \sin\theta. \tag{46}$$

Since in the sample-tilting scattering geometry, $(\pm)$ can be expressed as $(\tau\xi)$ for the first-order satellite ($\tau = \pm\xi$), Eq. (46) can be expressed as

$$(I_+ - I_-)^{(x\text{-}z)}_{\text{mag}} = (\tau\xi)\mathcal{D}^{(x\text{-}z)}_{\text{mag}}, \tag{47}$$

where the term $\mathcal{D}^{(x\text{-}z)}_{\text{mag}}$ is independent of both the diffraction order τ and the handedness of the helix ξ. The result of Eq. (47) is the behavior of CD-REXS for the chiral structure predicted by previous studies. The CD-REXS intensity for Néel-type helix of magnetic moments in sample-tilting scattering geometry is reversed when the sign of the diffraction order is reversed or the handedness of the helix is reversed.

Now, the results of Eqs. (45) and (47) for magnetic moments make it possible to distinguish a Bloch-type helix of (y-z) rotation showing true chirality from a Néel-type helix of (x-z) rotation corresponding to achiral structure, as shown in Fig. 2. This result is consistent with the previous result for the electric polarization vectors.

As discussed for electric polarization vectors, we can understand the results of Eqs. (45) and (47) intuitively by considering the mirrored situations. In the case of a Bloch-type helix of (y-z) plane rotation with $\xi = +1$ at the satellite peak with $\tau = +1$, the CD intensity is $(I_+ - I_-)^{(y\text{-}z)}_{\text{mag}} = \mathcal{B}^{(y\text{-}z)}_{\text{mag}}$ according to Eq. (45). In the mirrored image of the sample-tilting scattering geometry, the sign of the diffraction order τ of the lateral satellite is reversed ($\tau = -1$), as shown in Fig. 6, and in the mirrored Bloch-type helix, its handedness is also reversed ($\xi = -1$), as shown in Fig. 2. The CD intensity in the mirrored situation is then $(I_+ - I_-)^{(y\text{-}z)}_{\text{mag}} = -\mathcal{B}^{(y\text{-}z)}_{\text{mag}}$ according to Eq. (45). However, in the case of a Néel-type helix of (x-z) plane rotation with $\xi = +1$ at the satellite peak with $\tau = +1$, the CD intensity is $(I_+ - I_-)^{(x\text{-}z)}_{\text{mag}} = \mathcal{D}^{(x\text{-}z)}_{\text{mag}}$ according to Eq. (47). On the other hand, in the mirror situation, $\tau = -1$, but $\xi = +1$ as in Fig. 2, so the CD intensity is $(I_+ - I_-)^{(x\text{-}z)}_{\text{mag}} = -\mathcal{D}^{(x\text{-}z)}_{\text{mag}}$. These results are summarized in Table II.

Similarly to the electric polarization vectors, in both Bloch- and Néel-type helices with magnetic moments, the CD intensities in the mirror condition show the opposite sign of those in the original condition, as shown in Table II. This result is consistent with the fact that the helicity (or handedness) of circular polarization in the mirror situation is reversed compared to the original situation, as shown in Fig. 7. Therefore, in the sample-tilting scattering geometry, where the sign of the diffraction order τ is reversed in the mirrored situation and then it allows for discussion using the mirror reflection, the CD-REXS intensities for both electric polarization vectors and magnetic moments show a consistent behavior, as shown in Tables I and II.

TABLE II. Summary of the diffraction order τ, the handedness ξ, and the circular dichroism intensities for the original and mirrored helices with magnetic moments in the sample-tilting scattering geometry. Equations (45) and (47) correspond to Bloch-type and Néel-type helices, respectively.

	Original	Mirrored
Sample-tilting scattering geometry	$\tau = +1$	$\tau = -1$
Bloch-type helix with (y-z) plane rotation	$\xi = +1$	$\xi = -1$
$(I_+ - I_-)^{(y\text{-}z)}_{\text{mag}} = \xi\mathcal{B}^{(y\text{-}z)}_{\text{mag}}$ [Eq. (45)]	$+\mathcal{B}^{(y\text{-}z)}_{\text{mag}}$	$-\mathcal{B}^{(y\text{-}z)}_{\text{mag}}$
Néel-type helix with (x-z) plane rotation	$\xi = +1$	$\xi = +1$
$(I_+ - I_-)^{(x\text{-}z)}_{\text{mag}} = (\tau\xi)\mathcal{D}^{(x\text{-}z)}_{\text{mag}}$ [Eq. (47)]	$+\mathcal{D}^{(x\text{-}z)}_{\text{mag}}$	$-\mathcal{D}^{(x\text{-}z)}_{\text{mag}}$

Finally, the detailed evaluation of Eq. (34) using Eq. (31), which is the calculated REXS structure factor for magnetic moments in the sample-rocking scattering geometry, is given by

$$\frac{I_+ - I_-}{2} = |f_m|^2(-\sin(\theta_i + \theta_f)\cos\theta_f \ \text{Im}[\widetilde{\text{M}}^*_y\widetilde{\text{M}}_x] - \sin(\theta_i + \theta_f)\sin\theta_f \ \text{Im}[\widetilde{\text{M}}^*_y\widetilde{\text{M}}_z]). \tag{48}$$

First, we discuss a Bloch-type helix that rotates in the (y-z) plane. When all off-diagonal components of the AT $\boldsymbol{T}_0$ for the basis atom are zero and the magnetic structure factor $\widetilde{\text{M}}^{(y\text{-}z)}_i$ of Eq. (26) for first-order satellite ($\tau = \pm\xi$) is applied to Eq. (48), CD- REXS is given as

$$\frac{I_+ - I_-}{2} = \mp\frac{1}{4}|f_m|^2 \sin(\theta_i + \theta_f)\sin\theta_f. \tag{49}$$

Since $(\pm)$ can be expressed by $(\tau\xi)$ at the first-order satellite ($\tau = \pm\xi$), Eq. (49) can be expressed as

$$(I_+ - I_-)^{(y\text{-}z)}_{\text{mag-rock}} = (\tau\xi)\mathcal{D}^{(y\text{-}z)}_{\text{mag-rock}}, \tag{50}$$

where the term $\mathcal{D}^{(y\text{-}z)}_{\text{mag-rock}}$ is independent of both the diffraction order τ and the handedness of the helix ξ. Similarly, CD-REXS for a Néel-type helix rotating in the (x-z) plane for the first-order satellite ($\tau = \pm\xi$) can be obtained by applying Eq. (28) to Eq. (48) and is then given by

$$(I_+ - I_-)^{(x\text{-}z)}_{\text{mag-rock}} = 0. \tag{51}$$

because all terms in Eq. (48) contain $\widetilde{\text{M}}^{(x\text{-}z)}_y = 0$ in Eq. (28).

Equations (50) and (51) show that in the sample-rocking scattering geometry, the Bloch-type helix of the (y-z) plane rotation has a $(\tau\xi)$ dependence in CD-REXS intensity, while the Néel-type helix of (x-z) plane rotation has no CD in REXS. This behavior is the same as for CD-REXS from electric

TABLE III. Summary of the circular dichroism intensities for Bloch- and Néel-type helices with electrical polarization vectors and magnetic moments in the sample-rocking scattering geometry.

	Bloch-type helix with (y-z) plane rotation	Néel-type helix with (x-z) plane rotation
Electric polarization vectors	$(I_+ - I_-)^{(y\text{-}z)}_{\text{rock}} = (\tau\xi)\mathcal{D}^{(y\text{-}z)}_{\text{rock}}$ [Eq. (41)]	$(I_+ - I_-)^{(x\text{-}z)}_{\text{rock}} = 0$ [Eq. (42)]
Magnetic moments	$(I_+ - I_-)^{(y\text{-}z)}_{\text{mag-rock}} = (\tau\xi)\mathcal{D}^{(y\text{-}z)}_{\text{mag-rock}}$ [Eq. (50)]	$(I_+ - I_-)^{(x\text{-}z)}_{\text{mag-rock}} = 0$ [Eq. (51)]

polarization vectors in the sample-rocking scattering geometry. These results are summarized in Table III.

C. Simulations

In real systems, polar or magnetic helices emerge in an array form with a certain degree of disorder in ferroelectric superlattices or ferromagnetic domain walls. To describe quantitatively a degree of disorder in periodicity of helices, we introduce 1D paracrystal model [33,34]. When the paracrystal has a Gaussian distribution for the periodicity D with the width σ, the interference function due to a disordered array of helices can be given by

$$S_{\text{array}}(q_x) = \frac{1 - \tilde{g}(q_x)^2}{1 + \tilde{g}(q_x)^2 - 2\tilde{g}(q_x)\cos(q_x D)}, \tag{52}$$

where $\tilde{g}(q_x) = \exp[\pi q_x^2 \sigma^2]$. We note that all the CD intensities previously shown represent the calculations for the first-order satellite, where $q_x = 2\pi\tau/(N_x a)$ and $\tau = \pm 1$. Considering a disorder in the helicity period $D(= N_x a)$, the CD intensity distribution in the reciprocal space will be described as

$$(I_+ - I_-)(q_x) = (I_+ - I_-)_{\tau=\pm 1}\, S_{\text{array}}(q_x). \tag{53}$$

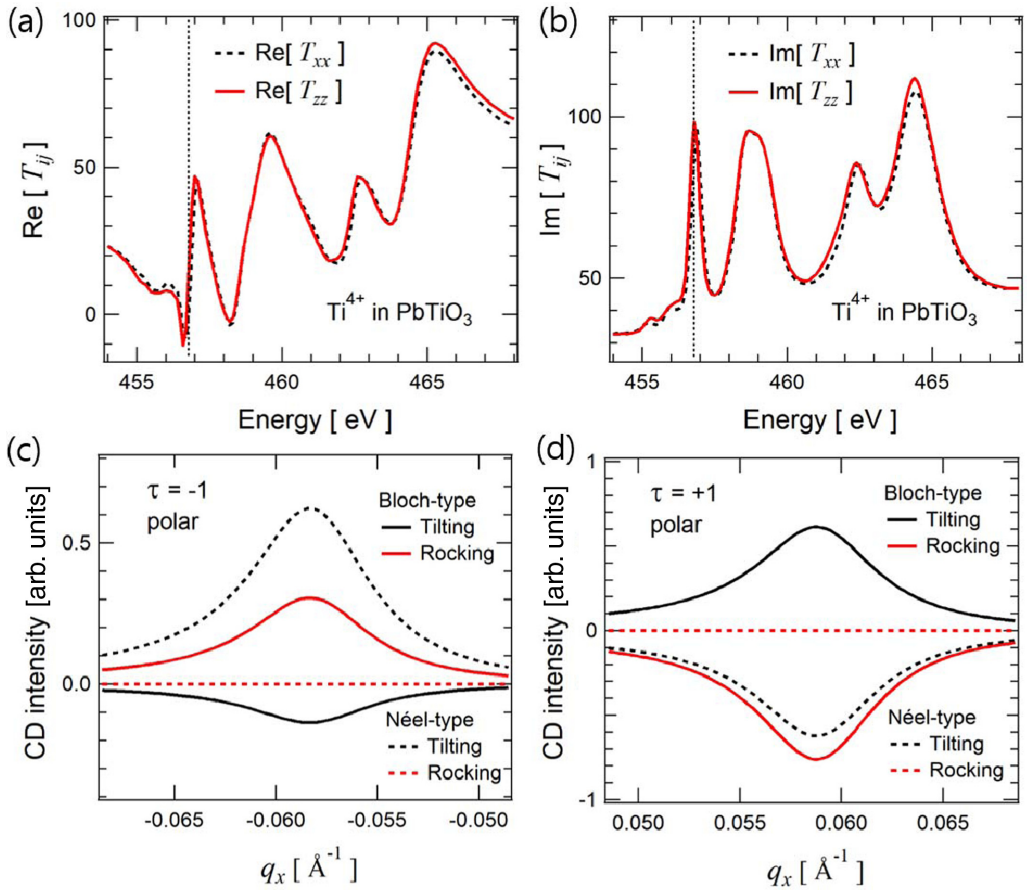

FIG. 9. (a), (b) Real and imaginary parts of the diagonal elements T_{xx} and T_{zz} in the AT of the basis atom Ti^{4+} in ferroelectric $PbTiO_3$. The energy dependences are shown aroundn the Ti $L_{2,3}$ edge. (c), (d) CD intensities for polar helices with Bloch- and Néel-type rotations in the sample-tilting and sample-rocking scattering geometries at the opposite satellite peaks ($\tau = \pm 1$). The energy was chosen as the Ti t_{2g} energy indicated by the vertical dotted lines in (a), (b). The lattice parameter $a = 3.94$ Å, the number of lattices in the unit cell of the helix $N_x = 28$, the period of the helicity $D \approx 11$ nm, and the handedness of the helicity $\xi = +1$, $\sigma/D = 0.1$, and $q_z = 0.2$ Å^{-1} were used for the calculations.

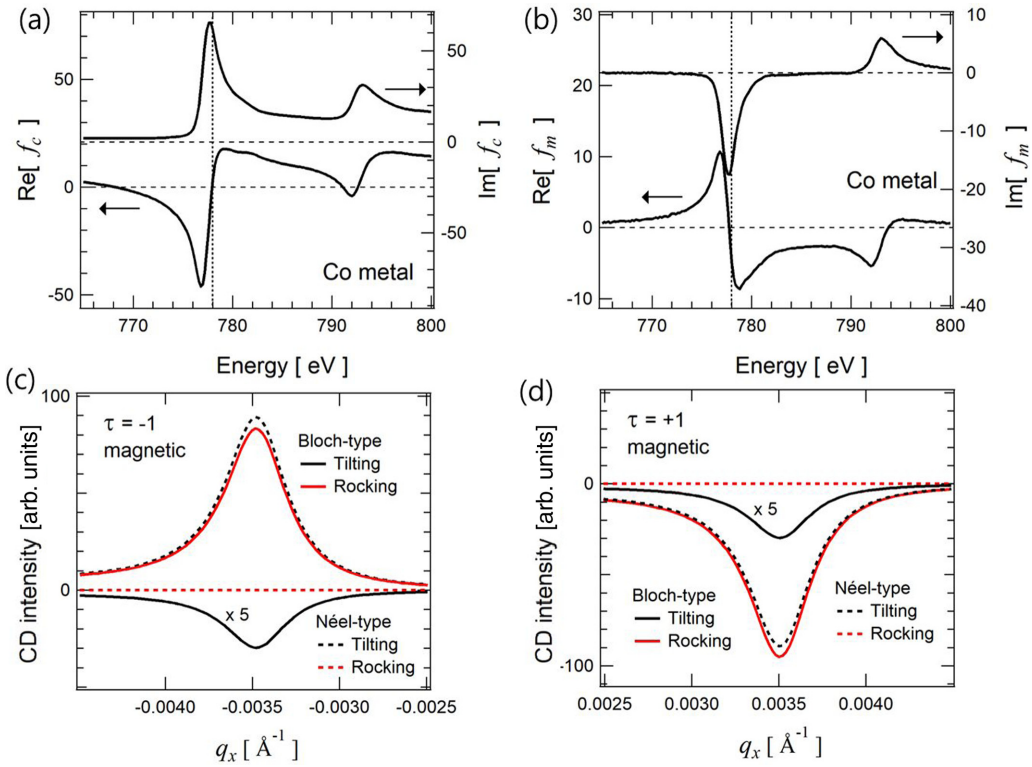

FIG. 10. (a), (b) Charge and magnetic atomic factors, f_c and f_m, across the Co $L_{2,3}$ edge for Co metal. (c), (d) CD intensities for magnetic helices with Bloch- and Néel-type rotations in the sample-tilting and sample-rocking scattering geometries at the opposite satellite peaks ($\tau = \pm 1$). The energy for the calculations is indicated by the vertical dotted lines in (a), (b). The lattice parameter $a = 3.48$ Å, the number of lattices in the unit cell of the helix $N_x = 517$, the period of the helicity $D \approx 180$ nm, and the handedness of the helicity $\xi = +1$, $\sigma/D = 0.1$, and $q_z = 0.2$ Å^{-1} were used for the calculations.

Figure 9 shows the simulated CD intensities for a polar helix. The energy-dependent AT values for Ti^{4+} ion in ferroelectric $PbTiO_3$ are shown in Figs. 9(a) and 9(b). The diagonal elements T_{xx} and T_{zz} in Eq. (3) for the basis atom have been obtained from the x-ray linear dichroism data [35]. Detailed values of other parameters used for the calculation are found in the figure caption. On the other hand, Fig. 10 shows the simulated CD intensities for a magnetic helix. The energy-dependent atomic factors, f_c and f_m, for Co metals are shown in Figs. 10(a) and 10(b). The period of magnetic helices typically observed in ferromagnetic domain walls is about hundreds of nanometers. On the other hand, the period of polar helices emerging in ferroelectric superlattices is an order of magnitude smaller than the magnetic one.

V. CONCLUSION

We have presented detailed analytic formulas of CD-REXS for two types of 1D helices, Bloch- and Néel-type helices, consisting of electric polarization vectors and magnetic moments. In particular, it has been shown in detail that a helix of electric polarization vectors has a completely different REXS structure factor from that for the magnetic moments, since not only the resonant scattering amplitude, which is an anisotropy tensor, but also an additional phase factor due to the displacement of the resonant atom itself should be considered. Interestingly, however, it was found that the CD-REXS intensities for the two types of helices show almost the same characteristics, despite the structure factors being different. In particular, CD-REXS intensity could discriminate Bloch- and Néel-type helices for both polar and magnetic vectors. We have also shown that not only the chiral structure itself but also the x-ray polarization factor depending on the scattering geometry is a significant cause of the characteristics of CD-REXS for the chiral structure. Therefore, based on this comprehensive understanding of CD-REXS, it is expected that an appropriate strategy can be established to elucidate the chiral structure appearing in polar, magnetic, or multiferroic thin films.

We have also shown that the characteristics of CD-REXS obtained quantitatively in various cases can be intuitively and consistently explained using mirror reflection. This method is not limited to the 1D helix discussed here but can also be applied to CD-REXS for 3D chiral structures. For example, in the case of a polar skyrmion composed of electric polarization vectors [6], the top and bottom parts have a Néel-type chiral structure while the middle part has a Bloch-type chiral structure. Therefore, by using the mirror reflection method, the characteristics of CD-REXS for this 3D chiral structure can be predicted intuitively.

ACKNOWLEDGMENTS

K.T.K., S.Y.P., and D.R.L. acknowledge financial support by National Research Foundation of Korea (Grants No. NRF-2020R1A2C1009597, No. NRF-2019K1A3A7A09033387,

and No. NRF-2021R1C1C1009494). We would like to thank Professor Stephen W. Lovesey for valuable discussions. The work at Berkeley is funded by the U.S. Department of Energy, Office of Science, Office of Basic Energy Sciences, Materials Sciences and Engineering Division under Contract No. DE-AC02-05-CH11231 within the Quantum Materials Program (No. KC2202). V.A.S. and J.W.F. acknowledge the U.S. Department of Energy, Office of Science, Office of Basic Energy Sciences, under Award No. DE-SC-0012375 for support to study complex-oxide heterostructures with X-ray scattering.

APPENDIX A: NO DISPLACEMENT ($\Delta = 0$) OF ELECTRICAL POLARIZATION VECTOR IN EQ. (14)

First, in Eq. (13), $\delta_{\xi}^{(y\text{-}z)}(x)$ is reduced to $\delta(x)$. In the case of (y-z) plane rotation, the helix-only structure factor $S_{ij}^{(y\text{-}z)}$ in Eq. (14) can be written as

$$
\begin{aligned}
S_{xx}^{(y\text{-}z)} &= T_{xx}\delta(\tau),\\
S_{yy}^{(y\text{-}z)} &= \frac{1}{4}\{2T_0\delta(\tau) + T_{2+}\delta(\tau+2\xi) + T_{2-}\delta(\tau-2\xi)\},\\
S_{zz}^{(y\text{-}z)} &= \frac{1}{4}\{2T_0\delta(\tau) - T_{2+}\delta(\tau+2\xi) - T_{2-}\delta(\tau-2\xi)\},\\
S_{xy}^{(y\text{-}z)} &= S_{yx}^{(y\text{-}z)} = \frac{1}{2}\{T_{1+}\delta(\tau+\xi) + T_{1-}\delta(\tau-\xi)\},\\
S_{xz}^{(y\text{-}z)} &= S_{zx}^{(y\text{-}z)} = \frac{1}{2i}\{T_{1+}\delta(\tau+\xi) - T_{1-}\delta(\tau-\xi)\},\\
S_{yz}^{(y\text{-}z)} &= S_{zy}^{(y\text{-}z)} = \frac{1}{4i}\{T_{2+}\delta(\tau+2\xi) - T_{2-}\delta(\tau-2\xi)\}. \qquad \text{(A1)}
\end{aligned}
$$

In the case of $\tau = \pm\xi$ corresponding to the first-order satellite, all components in Eq. (A1) become zero except the matrix components below:

$$
\begin{aligned}
S_{xy}^{(y\text{-}z)} &= S_{yx}^{(y\text{-}z)} = \tfrac{1}{2}(T_{xy} \mp iT_{xz}) = \tfrac{1}{2}[T_{xy} - (\tau\xi)(iT_{xz})],\\
S_{xz}^{(y\text{-}z)} &= S_{zx}^{(y\text{-}z)} = \tfrac{1}{2}(\mp T_{xy} + iT_{xz}) = \tfrac{1}{2}[-(\tau\xi)T_{xy} + iT_{xz}]. \qquad \text{(A2)}
\end{aligned}
$$

If the off-diagonal components of the basis atom are all zero, the matrix components of the helix-only structure factor $S_{ij}^{(y\text{-}z)}$ at the first-order satellite become all zero. These results are the same for a Néel-type helix with (x-z) plane rotation.

APPENDIX B: EVALUATION OF EQ. (35) FOR ELECTRICAL POLARIZATION VECTORS IN THE SAMPLE-TILTING SCATTERING GEOMETRY

The result of applying the structure factor in Eq. (30) for electrical polarization vectors to Eq. (35) for CD-REXS is

$$
\begin{aligned}
(I_+ - I_-)/2 &= \mathrm{Im}[F_{\sigma'\pi}^* F_{\sigma'\sigma} + F_{\pi'\pi}^* F_{\pi'\sigma}]\\
&= 2\cos\theta\cos^2\chi\sin^2\chi\,\mathrm{Im}[S_{xx}^* S_{xz}] - \cos\theta\cos\chi\sin^3\chi\,\mathrm{Im}[S_{xx}^* S_{zz}] - \sin\theta\cos^3\chi\,\mathrm{Im}[S_{xy}^* S_{xx}]\\
&\quad + 2\sin\theta\cos^2\chi\sin\chi\,\mathrm{Im}[S_{xy}^* S_{xz}] - \sin\theta\cos\chi\sin^2\chi\,\mathrm{Im}[S_{xy}^* S_{zz}] - \cos\theta\cos 2\chi\cos^2\chi\,\mathrm{Im}[S_{xz}^* S_{xx}]\\
&\quad - \cos\theta\cos 2\chi\sin^2\chi\,\mathrm{Im}[S_{xz}^* S_{zz}] + \sin\theta\sin\chi\cos^2\chi\,\mathrm{Im}[S_{yz}^* S_{xx}] - 2\sin\theta\cos\chi\sin^2\chi\,\mathrm{Im}[S_{yz}^* S_{xz}]\\
&\quad + \sin\theta\sin^3\chi\,\mathrm{Im}[S_{yz}^* S_{zz}] + \cos\theta\cos^3\chi\sin\chi\,\mathrm{Im}[S_{zz}^* S_{xx}] - 2\cos\theta\cos^2\chi\sin^2\chi\,\mathrm{Im}[S_{zz}^* S_{xz}]\\
&\quad - \cos^3\theta\sin^2\chi\cos 2\chi\,\mathrm{Im}[S_{xx}^* S_{xz}] + \cos^2\theta\sin\theta\sin^2\chi\cos\chi\,\mathrm{Im}[S_{xx}^* S_{xy}] - \cos^2\theta\sin\theta\sin^3\chi\,\mathrm{Im}[S_{xx}^* S_{yz}]\\
&\quad + \cos^3\theta\sin^3\chi\cos\chi\,\mathrm{Im}[S_{xx}^* S_{zz}] - 2\cos^3\theta\cos^2\chi\sin^2\chi\,\mathrm{Im}[S_{xz}^* S_{xx}]\\
&\quad + 2\cos^2\theta\sin\theta\cos^2\chi\sin\chi\,\mathrm{Im}[S_{xz}^* S_{xy}] - 2\cos^2\theta\sin\theta\cos\chi\sin^2\chi\,\mathrm{Im}[S_{xz}^* S_{yz}]\\
&\quad + 2\cos^3\theta\cos^2\chi\sin^2\chi\,\mathrm{Im}[S_{xz}^* S_{zz}] + \sin^2\theta\cos\theta\cos\chi\sin\chi\,\mathrm{Im}[S_{yy}^* S_{xx}]\\
&\quad + \sin^2\theta\cos\theta\cos 2\chi\,\mathrm{Im}[S_{yy}^* S_{xz}] - \sin^3\theta\cos\chi\,\mathrm{Im}[S_{yy}^* S_{xy}] + \sin^3\theta\sin\chi\,\mathrm{Im}[S_{yy}^* S_{yz}]\\
&\quad - \sin^2\theta\cos\theta\cos\chi\sin\chi\,\mathrm{Im}[S_{yy}^* S_{zz}] - \cos^3\theta\cos^3\chi\sin\chi\,\mathrm{Im}[S_{zz}^* S_{xx}] - \cos^3\theta\cos^2\chi\cos 2\chi\,\mathrm{Im}[S_{zz}^* S_{xz}]\\
&\quad + \mathrm{Im}[S_{zz}^* S_{xy}] - \cos^2\theta\sin\theta\cos^2\chi\sin\chi\,\mathrm{Im}[S_{zz}^* S_{yz}]. \qquad \text{(B1)}
\end{aligned}
$$

APPENDIX C: EVALUATION OF EQ. (35) FOR ELECTRICAL POLARIZATION VECTORS IN THE SAMPLE-ROCKING SCATTERING GEOMETRY

The result of applying the structure factor in Eq. (33) for electrical polarization vectors to Eq. (35) for CD is

$$
\begin{aligned}
(I_+ - I_-)/2 &= \mathrm{Im}[F_{\sigma'\pi}^* F_{\sigma'\sigma} + F_{\pi'\pi}^* F_{\pi'\sigma}]\\
&= \sin\theta_i\,\mathrm{Im}[S_{xy}^* S_{yy}] + \cos\theta_i\,\mathrm{Im}[S_{yz}^* S_{yy}] + \sin\theta_i\sin^2\theta_f\,\mathrm{Im}[S_{xx}^* S_{xy}] - \sin\theta_i\sin\theta_f\cos\theta_f\,\mathrm{Im}[S_{xx}^* S_{yz}]\\
&\quad - \cos\theta_f\sin\theta_f\cos\theta_i\,\mathrm{Im}[S_{zz}^* S_{xy}] + \cos^2\theta_f\cos\theta_i\,\mathrm{Im}[S_{zz}^* S_{yz}] - \sin 2\omega\sin\theta_f\,\mathrm{Im}[S_{xz}^* S_{xy}] + \sin 2\omega\cos\theta_f\,\mathrm{Im}[S_{xz}^* S_{yz}]. \qquad \text{(C1)}
\end{aligned}
$$

[1] A. Fert, N. Reyren, and V. Cros, Nat. Rev. Mater. **2**, 17031 (2017).

[2] W. Jiang, G. Chen, K. Liu, J. Zang, S. G. te Velthuis, and A. Hoffmann, Phys. Rep. **704**, 1 (2017).

[3] R. Tomasello, E. Martinez, R. Zivieri, L. Torres, M. Carpentieri, and G. Finocchio, Sci. Rep. **4**, 6784 (2015).

[4] A. Fert, V. Cros, and J. Sampaio, Nat. Nanotechnol. **8**, 152 (2013).

[5] X. Yu, N. Kanazawa, W. Zhang, T. Nagai, T. Hara, K. Kimoto, Y. Matsui, Y. Onose, and Y. Tokura, Nat. Commun. **3**, 988 (2012).

[6] S. Das, Y. L. Tang, Z. Hong, M. A. P. Gonçalves, M. R. McCarter, C. Klewe, K. X. Nguyen, F. Gómez-Ortiz, P. Shafer, E. Arenholz, V. A. Stoica, S.-L. Hsu, B. Wang, C. Ophus, J. F. Liu, C. T. Nelson, S. Saremi, B. Prasad, A. B. Mei, D. G. Schlom *et al.*, Nature (London) **568**, 368 (2019).

[7] J. P. Hannon, G. T. Trammell, M. Blume, and D. Gibbs, Phys. Rev. Lett. **61**, 1245 (1988).

[8] E. Dudzik, S. S. Dhesi, H. A. Dürr, S. P. Collins, M. D. Roper, G. van der Laan, K. Chesnel, M. Belakhovsky, A. Marty, and Y. Samson, Phys. Rev. B **62**, 5779 (2000).

[9] H. A. Durr, E. Dudzik, S. S. Dhesi, J. B. Goedkoop, G. van der Laan, M. Belakhovsky, C. Mocuta, A. Marty, and Y. Samson, Science **284**, 2166 (1999).

[10] W. Legrand, J.-Y. Chauleau, D. Maccariello, N. Reyren, S. Collin, K. Bouzehouane, N. Jaouen, V. Cros, and A. Fert, Sci. Adv. **4**, eaat0415 (2018).

[11] J.-Y. Chauleau, W. Legrand, N. Reyren, D. Maccariello, S. Collin, H. Popescu, K. Bouzehouane, V. Cros, N. Jaouen, and A. Fert, Phys. Rev. Lett. **120**, 037202 (2018).

[12] S. L. Zhang, G. van der Laan, W. W. Wang, A. A. Haghighirad, and T. Hesjedal, Phys. Rev. Lett. **120**, 227202 (2018).

[13] J.-Y. Chauleau, T. Chirac, S. Fusil, V. Garcia, W. Akhtar, J. Tranchida, P. Thibaudeau, I. Gross, C. Blouzon, A. Finco, M. Bibes, B. Dkhil, D. D. Khalyavin, P. Manuel, V. Jacques, N. Jaouen, and M. Viret, Nat. Mater. **19**, 386 (2020).

[14] G. van der Laan, C. R. Phys. **9**, 570 (2008).

[15] P. Shafer, P. García-Fernández, P. Aguado-Puente, A. R. Damodaran, A. K. Yadav, C. T. Nelson, S.-L. Hsu, J. C. Wojdeł, J. Íñiguez, L. W. Martin, E. Arenholz, J. Junquera, and R. Ramesh, Proc. Natl. Acad. Sci. USA **115**, 915 (2018).

[16] S. W. Lovesey and G. van der Laan, Phys. Rev. B **98**, 155410 (2018).

[17] W. Li, I. Bykova, S. Zhang, G. Yu, R. Tomasello, M. Carpentieri, Y. Liu, Y. Guang, J. Gräfe, M. Weigand, D. M. Burn, G. van der Laan, T. Hesjedal, Z. Yan, J. Feng, C. Wan, J. Wei, X. Wang, X. Zhang, H. Xu *et al.*, Adv. Mater. **31**, 1807683 (2019).

[18] A. K. Yadav, C. T. Nelson, S. L. Hsu, Z. Hong, J. D. Clarkson, C. M. Schlepütz, A. R. Damodaran, P. Shafer, E. Arenholz, L. R. Dedon, D. Chen, A. Vishwanath, A. M. Minor, L. Q. Chen, J. F. Scott, L. W. Martin, and R. Ramesh, Nature (London) **530**, 198 (2016).

[19] A. R. Damodaran, J. D. Clarkson, Z. Hong, H. Liu, A. K. Yadav, C. T. Nelson, S.-L. Hsu, M. R. McCarter, K.-D. Park, V. Kravtsov, A. Farhan, Y. Dong, Z. Cai, H. Zhou, P. Aguado-Puente, P. García-Fernández, J. Íñiguez, J. Junquera, A. Scholl, M. B. Raschke *et al.*, Nat. Mater. **16**, 1003 (2017).

[20] S. Das, A. Ghosh, M. R. McCarter, S.-L. Hsu, Y.-L. Tang, A. R. Damodaran, R. Ramesh, and L. W. Martin, APL Mater. **6**, 100901 (2018).

[21] S.-L. Hsu, M. R. McCarter, C. Dai, Z. Hong, L.-Q. Chen, C. T. Nelson, L. W. Martin, and R. Ramesh, Adv. Mater. **31**, 1901014 (2019).

[22] D. H. Templeton and L. K. Templeton, Acta Crystallogr., Sect. A: Found. Crystallogr. **38**, 62 (1982).

[23] V. E. Dmitrienko, Acta Crystallogr., Sect. A: Found. Crystallogr. **39**, 29 (1983).

[24] S. L. Zhang, G. van der Laan, and T. Hesjedal, Phys. Rev. B **96**, 094401 (2017).

[25] M. Blume, *Resonant Anomalous X-Ray Scattering: Theory and Applications*, edited by G. Materlik, C. J. Sparks, and K. Fischer (Elsevier Science B. V., Amsterdam, The Netherlands, 1994)

[26] K. T. Kim, M. R. McCarter, V. A. Stoica, S. Das, C. Klewe, E. P. Donoway, D. M. Burn, P. Shafer, F. Rodolakis, M. A. P. Gonçalves, F. Gómez-Ortiz, J. Íñiguez, P. García-Fernández, J. Junquera, S. Susarla, S. W. Lovesey, G. van der Laan, S. Y. Park, L. W. Martin, J. W. Freeland *et al.*, Nat. Commun. **13**, 1769 (2022).

[27] G. van der Laan, Phys. Rev. Lett. **82**, 640 (1999).

[28] D.-M. Smilgies, P. Busch, C. M. Papadakis, and D. Posselt, Synchrotron Radiat. News **15**, 35 (2002).

[29] G. Renaud, R. Lazzari, C. Revenant, A. Barbier, M. Noblet, O. Ulrich, F. Leroy, J. Jupille, Y. Borensztein, C. R. Henry, J.-P. Deville, F. Scheurer, J. Mane-Mane, and O. Fruchart, Science **300**, 1416 (2003).

[30] B. Lee, I. Park, J. Yoon, S. Park, J. Kim, K.-W. Kim, T. Chang, and M. Ree, Macromolecules **38**, 4311 (2005).

[31] S. Narayanan, D. R. Lee, R. S. Guico, S. K. Sinha, and J. Wang, Phys. Rev. Lett. **94**, 145504 (2005).

[32] J. Fernández-Rodríguez, S. W. Lovesey, and J. A. Blanco, Phys. Rev. B **77**, 094441 (2008).

[33] R. Hosemann and S. N. Bagchi, Acta Crystallogr. **5**, 612 (1952).

[34] R. Lazzari, *X-ray and Neutron Reflectivity*, edited by J. Daillant and A. Gibaud (Springer, Berlin, Heidelberg, 2009), Vol. 770, pp. 283–342.

[35] E. Arenholz, G. van der Laan, A. Fraile-Rodríguez, P. Yu, Q. He, and R. Ramesh, Phys. Rev. B **82**, 140103(R) (2010).